Mechanical Systems and Signal Processing 224 (2025) 112012

Contents lists available at ScienceDirect

Mechanical Systems and Signal Processing

journal homepage: www.elsevier.com/locate/ymssp

Piezoelectric coupling as a feature sensitive to structural alterations

M. Berardengo [a], M. Brambilla [b], A. Codina [b], N. Schena [b], S. Manzoni [b,*]

[a] Università degli Studi di Genova - Department of Mechanical, Energy, Management and Transportation Engineering, Via all'Opera Pia, 15A - 16145 Genoa, Italy

[b] Politecnico di Milano - Department of Mechanical Engineering, Via La Masa, 1 - 20156 Milan, Italy

ARTICLE INFO

Communicated by M. Brake

Keywords:
Piezoelectric elements
Piezoelectric structure
Electro-mechanical coupling factor
Negative capacitance
Structural monitoring
Piezoelectric shunt

ABSTRACT

The paper presents an exploratory study about the use of electro-mechanical coupling measurements as a feature for detecting structural alterations using piezoelectric transducers. This coupling between the piezoelectric transducers and the structure can be estimated by means of low frequency vibration measurements and will prove to be a feature sensitive to structure alterations and scarcely influenced by temperature variations. Moreover, the approach proposed is designed such that it can also employ piezoelectric elements already available in the system for other purposes (e.g., vibration control), thus not requiring any additional expensive device, and can work while the system to be monitored is operating.

The paper introduces at first the principle of the method and shows how to improve its accuracy by connecting the piezoelectric transducers with proper electric impedances. Then, numerical simulations and experimental results are presented to prove the feasibility of the proposed approach.

1. Introduction

Structural health monitoring (SHM) is a discipline widely studied nowadays, with the aim of finding reliable methods and approaches to detect damages in machinery, systems and structures. Considering light structures (e.g., space truss structures, blades, wing panels, cable structures), they often show significant vibration levels just because of their low weight and this makes natural the measurement of these vibrations for the purpose of their monitoring. Indeed, among the different existing approaches for monitoring light structures, a significant number of them is based on the measurement of the dynamics of the system under analysis in terms of, as examples, dynamic acceleration and strain since this allows for monitoring the system in operating conditions. In the class of vibration-based methods [1], there are some based on the monitoring of the trend of some indexes directly derived from vibration data (e.g., [2]) and others which monitor system modal data (e.g., mode shapes) extracted from the measured vibration signals (e.g., [3–6]). Other approaches use, instead, the obtained modal data as input to some mathematical procedures (e.g., [7–10]), or model-based techniques (e.g., [11–13]).

This paper aims at presenting an exploratory study on a method that can be seen as part of the class of vibration-based methods and which relies on the measurement of the coupling between piezoelectric transducers present in the system to be monitored and the system itself. Indeed, it will be proven that this electro-mechanical coupling is a feature sensitive to system alterations and robust to possible changes of the environmental and operating conditions.

In the field of structural monitoring, piezoelectric elements have already been used as sensors (e.g., [14]), or to enhance the sensitivity to the damage [15], or in the context of the electro-mechanical impedance (EMI) technique (e.g., [16–18]) where

* Corresponding author.
E-mail address: stefano.manzoni@polimi.it (S. Manzoni).

https://doi.org/10.1016/j.ymssp.2024.112012
Received 24 December 2023; Received in revised form 25 August 2024; Accepted 1 October 2024

the structural alterations are correlated to the measurement of the current flowing through the piezoelectric element attached to the structure as a result of the applied voltage to it, or vice versa. Here, piezoelectric transducers are employed in a different way: when a piezoelectric transducer is integrated in a structure, its sensing and actuating capabilities depend on the coupling between the structure and the piezoelectric transducer, named electro-mechanical coupling factor. This parameter is related to the values of the system mode shapes at the piezoelectric transducer location and, thus, it is sensitive to their changes due to possible structural alterations [19]. It will thus be considered here as a possible clue of structural alterations. However, the estimation of the electro-mechanical coupling factor does not rely on the estimation of mode shapes and thus, unlike the case of mode shapes, its estimation is easier and characterised by a lower level of uncertainty because its value can be found through the measurement of the eigenfrequencies of the coupled system. Furthermore, this approach allows working in the low frequency range (i.e., up to few kilohertz, unlike EMI techniques which mainly work at high frequency, hundreds of kilohertz or more [20]), which implies significant advantages as evidenced in this study.

The use of coupling measurements for SHM purposes has never been studied and validated till now. Therefore, the proposed damage feature (i.e., electro-mechanical coupling factor) will not be compared here with other features/methods available in the literature in terms of performances. In this paper, only a feasibility study will be shown to evaluate the potentialities of the approach and to define if it is worthy of further investigations. However, it is important to evidence that an approach based on the proposed damage feature has various advantages if compared to other SHM methods:

- the method can employ, for SHM, piezoelectric transducers already present in the structure for other purposes since they usually show high coupling values (high coupling is required for, e.g., vibration control purposes);
- the considered damage feature (i.e., the electro-mechanical coupling factor) will prove to be robust to environmental and operational conditions and related to the distance between the damage and the transducer;
- the frequency range of the vibration measurements needed for the method allows avoiding the use of high-performance acquisition boards or other expensive devices. Therefore, the proposed approach foresees a simple procedure and relies on simple vibration measurements.

According to the above bulleted list, the proposed damage feature can be seen as the base of a new monitoring approach, but also as a support tool either in situations where no monitoring system is present in the considered structure or to provide inputs to already existing monitoring systems by giving information slightly affected by operational and environmental effects and somehow connected to the distance between the damage and the transducer. This is another reason why here the main purpose is to study the potentialities of the electro-mechanical coupling as damage feature, without comparing the use of this feature as a stand-alone monitoring method against other SHM approaches. This paper is thus intended as an exploratory study for comprehending peculiarities, practical applicability and reliability of the use of electro-mechanical coupling factor measurement as a damage feature. Indeed, the paper also addresses the feasibility of the accurate identification of the quantities to be derived to estimate the electro-mechanical coupling from the measured data, since they can be small and their estimation could be affected by a non-negligible uncertainty.

It is underlined that the generic term alteration is used here (in place of the specific term damage) because, as shown further in the paper, any type of structural modification involving a significant mode shape change can be considered, as, for example, malfunction of micro-electro-mechanical sensors. Indeed, micro-electro-mechanical sensors based on a flexible beam can use a piezoelectric patch with the aim of tuning the frequency band of the sensor itself, by changing the dynamics of the beam. Being the device at the micro scale, it could occur that undesired dust or other materials appearing on the beam could affect the behaviour of the sensor. The diagnostic method presented herein could be used also in this case to detect the presence of the extraneous material affecting the proper functioning of the device.

The paper is structured as follows: Section 2 presents the model used to describe the electro-mechanical behaviour of the coupled system, the working principle of the proposed detection method and the quantities to be measured for the monitoring. Then, Section 3 discusses the uncertainty affecting the method results, showing how to improve it by connecting a proper electric impedance to the piezoelectric elements, Section 4 investigates method sensitivity to environmental and operational conditions and Section 5 presents the strengths of the approach and the operative procedure to use it. Then, numerical simulations and experiments are described in Sections 6 and 7, respectively, to show the feasibility of the approach and validate its working principle. Finally, Section 8 summarises the most relevant aspects related to the newly proposed damage feature.

2. The model of the system and the diagnostic method

This section aims at presenting, at first, the model used to describe the dynamics of the electro-mechanical system. This model allows introducing the proposed diagnostic index and the quantities involved in its estimation. Then, in next sections, the use of the index to SHM purposes will be presented and discussed in detail.

2.1. The model of the electro-mechanical system and the foundations of the monitoring strategy

A generic structure excited by an external force F and connected with a given number (one or more) of piezoelectric transducers (either patches or stacks) is considered. In this subsection, the configuration of Fig. 1 consisting in a single piezoelectric patch is taken into account for the sake of conciseness, without any loss of generality. Indeed, the analytical treatment and the proposed

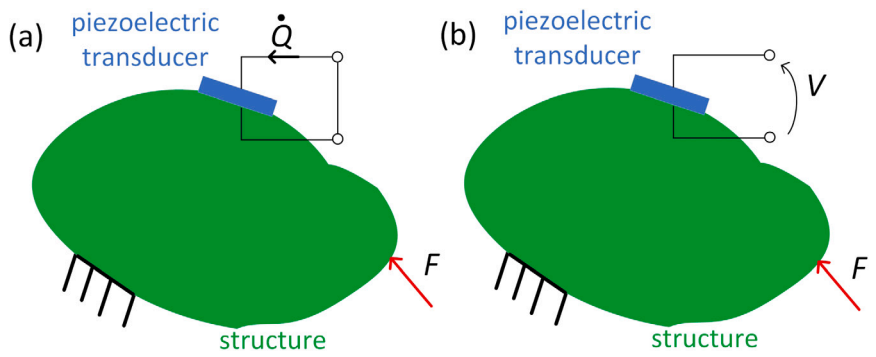

Fig. 1. A piezoelectric transducer bonded to a vibrating structure in short- (a) and open-circuit (b).

monitoring method can be easily extended to the case of piezoelectric stacks and of more than one transducer, as also evidenced in Sections 6 and 7. The electro-mechanical system (EMS, i.e., the global system composed by the main structure and the piezoelectric transducers) can be modelled with a modal approach [21], enabling to describe the dynamics of the whole system in the frequency range of interest. The mentioned modal model can be expressed in terms of the modal coordinates q_i and the eigenvectors ϕ_i of the system, scaled to the unit modal mass, with the piezoelectric transducer short-circuited (i.e., with $V = 0$, being V the voltage across the electrodes of the piezoelectric patch, see Fig. 1). The equation of motion of the EMS and the electrical behaviour of the piezoelectric transducer can be expressed, respectively, as:

$$\ddot{q}_i + 2\xi_i\omega_i\dot{q}_i + \omega_i^2 q_i - \chi_i V = F_i \quad \forall i = 1, \dots, N \tag{1}$$

$$C_\infty V - Q + \sum_{i=1}^{N} \chi_i q_i = 0 \tag{2}$$

where a single dot and a pair of dots represent the first and second time derivative, respectively, and N is the number of modes of the EMS and, theoretically, N tends to ∞. Furthermore, ω_i is the ith eigenfrequency of the EMS with the piezoelectric patch short-circuited, ξ_i is the associated non-dimensional damping ratio and F_i is the modal forcing. The variable C_∞ indicates the capacitance of the piezoelectric patch with the blocked structure, which also corresponds to the capacitance at infinite frequency [22]. Furthermore, Q is the charge in one of the two electrodes ($-Q$ in the other) and χ_i is a modal coupling coefficient which describes the energy transfer between the piezoelectric patch and the ith mode.

If only the ith mode is considered in a reduced model, the mechanical behaviour is described by Eq. (1) written only for the ith mode and the electrical equation, Eq. (2), can be written as [22]:

$$C_{\mathrm{p}i} V - Q + \chi_i q_i = 0 \tag{3}$$

where $C_{\mathrm{p}i}$ is the modal capacitance of the ith mode. The use of $C_{\mathrm{p}i}$ in place of C_∞ allows taking into consideration the static contribution of the modes higher than the ith, which are neglected in the reduced model. The contribution of the modes lower than the ith usually tends to be negligible [22,23]. $C_{\mathrm{p}i}$ can be roughly seen as the capacitance of the piezoelectric patch at frequency values between the ith and the $(i+1)$-th eigenfrequencies. More details about the estimation and the meaning of $C_{\mathrm{p}i}$ can be found in [22–24].

When the piezoelectric patch is open-circuited (i.e., $Q = 0$, see Fig. 1), the expression of V as a function of the modal coordinates can be found through Eq. (3), and substituting it in Eq. (1) leads to:

$$\ddot{q}_i + 2\xi_i\omega_i\dot{q}_i + (\omega_i^2 + \frac{\chi_i^2}{C_{\mathrm{p}i}})q_i = F_i \tag{4}$$

Eq. (4) shows that the open-circuit eigenfrequency of the EMS, named here $\hat{\omega}_i$, is different from that in short-circuit (i.e., ω_i) and its expression is:

$$\hat{\omega}_i^2 = \omega_i^2 + \frac{\chi_i^2}{C_{\mathrm{p}i}} \tag{5}$$

This results in having $\hat{\omega}_i$ higher than ω_i, and thus the open-circuit condition implies a stiffening effect on the EMS, whose extent depends on the value of the term χ_i. It can be demonstrated that the modal coupling coefficient χ_i depends on two terms: γ and ψ_i [25,26], where γ is a function of the geometrical, mechanical and electrical features of the mechanical structure and the piezoelectric transducer (e.g., Young's modules, piezoelectric strain constants) and ψ_i is a term depending on the position of the piezoelectric transducer on the mechanical structure.

Achieving high values of γ and ψ_i implies to obtain a high value of χ_i. Therefore, in applications where piezoelectric transducers are used, the γ and ψ_i terms are made as high as possible by properly choosing the features of the piezoelectric transducer and its

position on the structure because this improves the performances of the piezoelectric device (e.g., the attenuation performance in case of vibration control, the energy conversion in case of energy harvesting) through an increase of the efficiency of the electro-mechanical conversion (i.e., increase of the absolute value of χ_i). The analytical expressions of γ and ψ_i depend on the specific structure considered. However, some general considerations can be made regarding these two parameters. As for γ, it depends, as mentioned, on the geometrical, mechanical and electrical properties of the piezoelectric element and the structure. Particularly, γ depends on the ratios between the values of different parameters of the piezoelectric element and the structure (e.g., ratio of Young's modules, ratio of thickness values). Examples for beam- and plate-like structures can be found in [25,27]. This suggests that possible changes of the structure dimensions (e.g., thickness, length) or material modifications (e.g., Young's modulus changes due to oxidation, chemical alterations, etc.) will affect the γ value and thus the coupling between the piezoelectric transducer and the structure. Instead, as for the term ψ_i, it depends on the slope of the mode shapes at the boundaries of the piezoelectric patch. As an example, for mono-dimensional structures (e.g., beams), its expression is [25]:

$$\psi_i = \phi_i'(x_2) - \phi_i'(x_1) \tag{6}$$

where ϕ_i' is the first derivative of ϕ_i with respect to the coordinate x along the beam length, and x_1 and x_2 are the coordinate values of the boundaries of the piezoelectric patch. Therefore, the physical meaning of ψ_i is the difference of the mode shape slopes at the boundaries of the piezoelectric patch. For bi-dimensional structures (e.g., plates), the expression of ψ_i becomes more complicated [27] but its meaning is still related to the mode shape slope at the boundaries of the piezoelectric patch. Therefore, it is possible to conclude that the value of χ_i is related to the EMS mode shapes and, in case a mode shape changes at the boundaries of the piezoelectric patch due to a structural alteration, the corresponding value of χ_i changes as well. This suggests that the monitoring of the trend of χ_i can be a tool for detecting a structural alteration, since such an alteration is able to affect both γ and ψ_i. Therefore, this approach can be somehow included in the category of methods based on mode shapes, which is shown to be effective for damage detection (e.g., [28–30]), or indexes dependent on mode shapes (e.g., [31,32]).

However, the estimation of χ_i is not straightforward and, thus, a different index, related to χ_i and easier to be estimated, needs to be found to the aim of structural monitoring. To this purpose, rearranging Eq. (5), it is possible to notice that $\hat{\omega}_i$ can be expressed as a function of the modal electro-mechanical coupling factor k_i:

$$\hat{\omega}_i^2 = \omega_i^2(1 + k_i^2) \tag{7}$$

where

$$k_i^2 = \frac{\chi_i^2}{\omega_i^2 C_{\mathrm{p}i}} \tag{8}$$

Rearranging Eq. (7), it is possible to express $|k_i|$ as a function of the short-, ω_i, and open-circuit, $\hat{\omega}_i$, eigenfrequencies:

$$|k_i| \simeq \sqrt{\frac{\hat{\omega}_i^2 - \omega_i^2}{\omega_i^2}} \tag{9}$$

The symbol $\simeq$ is used to indicate that the exact equality is valid just in case of null additional influence of the modes different from the ith in the reduced model. In case of significant modal superimposition, the relation of Eq. (9) represents an approximation of the actual $|k_i|$ value. $|k_i|$ can be seen as a normalised measure of the efficiency of the electro-mechanical conversion for the ith mode (e.g., [33]).

According to Eq. (8), k_i is proportional to χ_i and, thus, it is a function of ψ_i as well. This implies that a mode shape change will also affect the value of $|k_i|$. Furthermore, Eq. (9) shows that $|k_i|$ can be easily estimated by means of modal analyses providing estimates of ω_i and $\hat{\omega}_i$. Therefore, Eqs. (8) and (9) suggest that changes of mode shapes due to structural alterations can be detected by monitoring the trend of $|k_i|$, thus measuring the short- (ω_i) and open-circuit ($\hat{\omega}_i$) eigenfrequencies of the whole system.

Considering the discussion carried out so far, the use of k_i as damage feature in SHM algorithms can be associated to methods relying on mode shapes. However, unlike these methods, the proposed approach, although affected by mode shape changes, does not rely on their estimation. This represents a relevant difference with respect to traditional SHM methods based on mode shapes, and an advantage as well. Indeed, considering approaches based on mode shapes, they often require a dense mesh to measure the mode shape and, thus, several dedicated sensors are usually needed. Furthermore, they often suffer of problems related to, e.g., noise effects. Conversely, here, the procedure is based on eigenfrequency estimates, which can be obtained using a low number of sensors (even one transducer), are affected by lower uncertainty and can be often carried out easily also in operational conditions. The use of k_i as damage feature, thus, opens to the possibility of employing also transducers usually used for applications different from SHM, without the need of several additional dedicated sensors. Furthermore, being this approach based on mode shape changes, its damage sensitivity is of the same order of magnitude of other methods available in the literature and based on the estimation of mode shapes (or related quantities such as, e.g., curvature). Moreover, it is worth underling that the electro-mechanical coupling is also affected by changes in geometrical and mechanical properties, through the parameter γ, thus possibly increasing its sensitivity to alterations.

2.2. The diagnostic index

Section 2.1 showed that the modal electro-mechanical coupling factor k_i can be used as a diagnostic parameter, whose monitoring can indicate structural alterations implying a change of γ and/or of the ith system mode shape (and, thus, of ψ_i). This parameter

can be theoretically monitored for all the modes of the structure and, when a system is equipped with more than one piezoelectric transducer, also for all the transducers. A possible way to monitor the trend of $|k_i|$ is to estimate the percentage change of its value, $\Delta_{i,p}$, for each considered transducer p:

$$\Delta_{i,p} = \left| \frac{|k_{i,p,\mathrm{a}}| - |k_{i,p}|}{|k_{i,p}|} \right| \times 100 \tag{10}$$

where the subscript 'a' indicates the presence of the alteration, while absence of 'a' means that the system is in the reference condition, which is related to the $|k_i|$ value measured at the beginning of the system life or when its nominal/healthy condition is assured through other analyses. Estimating $\Delta_{i,p}$ on different modes allows increasing the statistical reliability of the analysis without increasing the complexity of the procedure. Indeed, all the $|k_i|$ values related to a transducer can be estimated simultaneously with only two modal analyses: one with the transducer short-circuited and the other with the transducer open-circuited (see Eq. (9)). It is important to notice that, when the $|k_i|$ of a transducer is estimated, all the other transducers must be always in the same condition (either short- or open-circuited).

However, despite the index of Eq. (10) can be a good parameter to track any change in the value of the modal electro-mechanical coupling factors, it must be considered that the $|k_i|$ values can be small quantities and, even if they are made as high as possible when the transducer type and location are optimised, it is not straightforward to have high $|k_i|$ values for all the modes. Small $|k_i|$ values imply short- and open-circuit eigenfrequencies close each other (see Eq. (9)) and this often translates into high uncertainty associated to the $|k_i|$ estimate [24,34,35]. This issue prevents an accurate estimation of $\Delta_{i,p}$ for modes with very low $|k_i|$ values since an unreliable $|k_i|$ estimate can lead to a high percentage change of $\Delta_{i,p}$, thus decreasing the reliability of the index. This pushes towards the use of a different index accounting for the information related to all the modes but, at the same time, giving low weight to the less reliable ones:

$$s_p = \sum_{i=1}^{N} \left| \left(|k_{i,p,\mathrm{a}}| - |k_{i,p}| \right) \right| \tag{11}$$

where the sum on the modes can be actually extended to the desired number of modes.

The use of the index s offers indeed two main advantages. The first, as mentioned, is that, in the summation, a mode with a low value of $|k_{i,p}|$, and thus characterised by a high uncertainty associated to its estimation, gives a negligible contribution to the index s. Furthermore, taking into consideration different modes together increases the robustness of the index because some modes can be affected by the presence of a given alteration in a given position of the structure, while others could not be affected. Therefore, an index based on as many modes as possible offers an increased statistical reliability.

An additional aspect related to the use of the index s concerns the possibility not only to detect the presence of an alteration but also to get information about its location. When a single piezoelectric transducer is present on the structure, s can be used only to find the presence of a possible alteration. As an example, this is the case in which piezoelectric elements are already installed for vibration control in small structures (e.g., turbine blades [36], composite panels [37] or small devices [38,39]). Instead, when larger structures are considered, the chance to have more than a single piezoelectric transducer is high (e.g., [40–43]) and this offers the possibility to get a first estimate of the location of the alteration. Indeed, an alteration is expected to modify the mode shapes especially in the vicinity of its location [44]. Therefore, a higher s index value is expected for those piezoelectric transducers placed close to the alteration. Although this is true when a high number of modes is used to calculate s, it could not subsist when a low number of modes is considered. Indeed, an alteration can sometime generate changes of some mode shapes even far from it [44], implying that the value of s could be high also for piezoelectric transducers far from the alteration, thus assuming values comparable to those associated to closer transducers when a small amount of modes is employed in the calculation of s. Therefore, to improve the reliability of the index s for detecting the position of the alteration, it is strongly suggested to increase as much as possible the number of modes considered. The use of s for the localisation of the alteration will be discussed again further in the paper.

3. Method reliability and sensitivity: uncertainty on the estimation of $|k_i|$

Section 2.2 evidenced the possibility of detecting structural alterations by monitoring a diagnostic index based on the estimate of the modal electro-mechanical coupling factors $|k_i|$. However, it has also been mentioned that the estimate of $|k_i|$ can be affected by a non-negligible uncertainty level, especially when the considered mode is characterised by a low $|k_i|$ value. Therefore, it is essential to evaluate the uncertainty on the $|k_i|$ estimates to assess the feasibility of the proposed diagnostic procedure and the possibility to ascribe changes in the index s to a structural alteration.

Before introducing a detailed quantification of the uncertainty associated to the estimation of $|k_i|$, a method able to increase the value of $|k_i|$ is presented in Section 3.1. It is based on the connection of a negative capacitance (NC) to the piezoelectric transducer. The possibility of increasing $|k_i|$ allows, indeed, for a significant decrease of the relative uncertainty on its estimate, as shown in Section 3.2, where the expressions to quantify the uncertainty are derived.

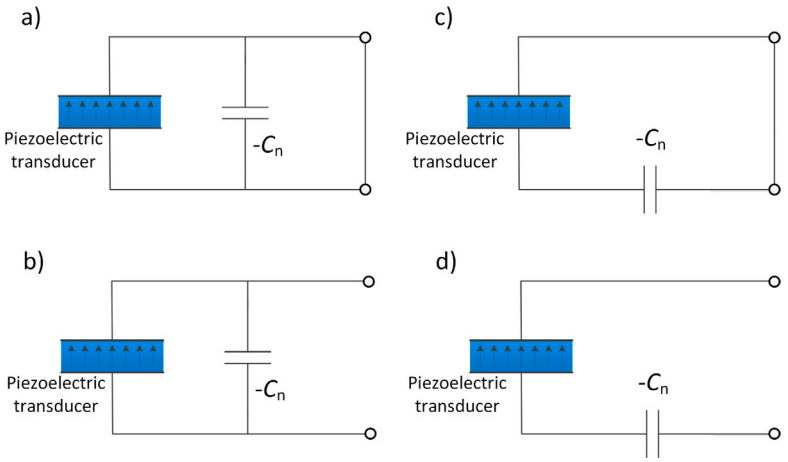

Fig. 2. A piezoelectric transducer connected in parallel to an NC in short-circuit (a) and open-circuit (b) configurations. A piezoelectric transducer connected in series to an NC in short-circuit (c) and open-circuit (d) configurations.

3.1. The use of an NC to increase the value of $|k_i|$

As mentioned, the higher the value of $|k_i|$ is, the lower the relative uncertainty associated to its estimation is, thus improving the accuracy of the diagnostic method. However, once the piezoelectric transducer type and its position on the structure are set, the value of $|k_i|$ is fixed. A possible way to artificially increase its value is to shunt the piezoelectric transducer with an NC, $-C_n$. NCs do not exist in nature but they can be built using operational amplifiers [45]. An NC can be connected to a piezoelectric transducer in either parallel (see Figs. 2a and b) or series (see Figs. 2c and d). Considering either the series or the parallel between the piezoelectric element and the NC as an equivalent enhanced transducer, it is possible to define new short- and open-circuit eigenfrequencies, according to Fig. 2. When the NC is connected in parallel, the new short-circuit eigenfrequencies do not change because the charge produced by the deflected piezoelectric patch always flows in the short-circuit branch and not in the branch with $-C_n$ (see Fig. 2a). Conversely, when the network is open-circuited (see Fig. 2b), it is evident that the presence of $-C_n$ affects the behaviour of the whole circuit because current flows through it. According to [22,46], this makes the new open-circuit eigenfrequencies shift towards higher frequency values compared to the open-circuit eigenfrequencies when the NC is not shunted. The new open-circuit eigenfrequencies will be referred to as ω_i^{oc}. When the NC is connected in series, the new open-circuit eigenfrequencies do not change because no current flows through $-C_n$ (see Fig. 2d). On the other hand, when the network is short-circuited (see Fig. 2c), the presence of $-C_n$ affects the behaviour of the whole circuit because current flows through it. According to [22,46], this makes the new short-circuit eigenfrequencies shift towards lower frequency values compared to the short-circuit eigenfrequencies when the NC is not added. The new short-circuit eigenfrequencies will be referred to as ω_i^{sc}.

In both the cases (parallel or series connection of the NC), the distance between the short- and open-circuit eigenfrequencies increase [22]. This new increased distance allows defining a modified equivalent $|k_i|$, which can be estimated, similarly to Eq. (9), as:

$$|\tilde{k}_i| \simeq \sqrt{\frac{(\omega_i^{oc})^2 - \omega_i^2}{\omega_i^2}} \tag{12}$$

for a parallel connection of the NC, and as:

$$|\tilde{k}_i| \simeq \sqrt{\frac{\hat{\omega}_i^2 - (\omega_i^{sc})^2}{(\omega_i^{sc})^2}} \tag{13}$$

for a series connection of the NC. In both the cases $|\tilde{k}_i| > |k_i|$. Here no details are provided about the use of NCs in piezoelectric shunt and just few important aspects for the considered applications are recalled. More details can be found in [22,47].

It is important to notice that the presence of an NC is able to increase the value of all the $|k_i|$ at the same time (i.e., for all the modes), thus resulting in an improved estimation for all the considered modes. However, it is not possible to have an unlimited increase of $|\tilde{k}_i|$ because of stability issues. Indeed, for an NC in parallel, the value of C_n must be lower than the value of C_∞ to assure the stability of the EMS. Considering an NC in series, the stability is assured when the value of C_n is higher than the value of the capacitance of the piezoelectric transducer at 0 Hz. The closer the value of C_n is to the stability limit, the higher the shifts of the eigenfrequencies will be and the higher the values of $|\tilde{k}_i|$ will be. Obviously, the presence of stability limits constraints the achievable $|k_i|$ increase.

Usually, a parallel NC is employed when it is important to make high the value of $|\tilde{k}_i|$ for high-frequency modes, while a series NC is adopted when it is important to make high the value of $|\tilde{k}_i|$ for low-frequency modes. When modes in the middle frequency

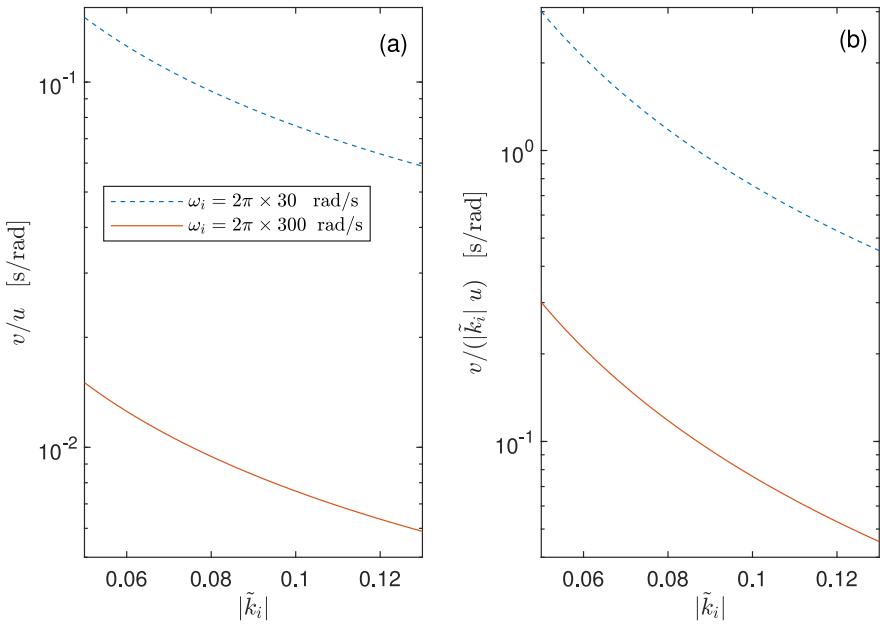

Fig. 3. Trend of v/u (a) and $v/(|\tilde{k}_i|\, u)$ (b) for a mode with either $\omega_i = 2\pi \times 30$ rad/s or $\omega_i = 2\pi \times 300$ rad/s. $|k_i| = 0.05$ in both the cases.

range are considered, both the NC configurations can be used, or a further configuration made from two NCs can be fruitfully employed [48,49]. Since the diagnostic method presented in this paper is expected to work with devices already present on the structure and/or usually operating in the low frequency range (few kilohertz or less), an NC in series will be considered from here on. However, the whole discussion can be extended to the parallel case as well.

Before ending this subsection, it also worth mentioning that another method exists for improving the reliability of the estimation of electro-mechanical coupling factors and it requires to shunt the piezoelectric element with an inductance [19,24]. Nevertheless, this method requires to tune the inductance for each mode (i.e., it does not allow lowering the estimation uncertainty on all the $|\tilde{k}_i|$ values at the same time). Thus, this further approach is not considered here.

3.2. Uncertainty quantification

This subsection aims at describing the uncertainty associated to the estimate of the modal electro-mechanical coupling factor. Here, the analysis is carried out considering the case where an NC in series is used to enhance the value of $|k_i|$ and thus the uncertainty associated to $|\tilde{k}_i|$ in Eq. (13) will be derived. Nevertheless, due to the similarity among Eqs. (12), (9) and (13), the same approach can be followed, with similar results, for deriving the uncertainty associated to the estimated $|\tilde{k}_i|$ and $|k_i|$ values in the cases of a parallel NC and when no NC is used, respectively.

The standard uncertainty v of $|\tilde{k}_i|$ can be described by means of the combined uncertainty formulation [50], which is based on a Taylor expansion. Here, the estimates of $\hat{\omega}_i$ and ω_i^{sc}, obtained through modal analyses, are assumed as independent and the standard uncertainty associated to the estimates is assumed equal and referred to as u. Assuming that the Taylor expansion can be truncated to the first order terms for the sake of simplicity, v assumes the following expression (refer to Eq. (13)):

$$v = \sqrt{\left(\frac{\partial|\tilde{k}_i|}{\partial\hat{\omega}_i}\right)^2 u^2 + \left(\frac{\partial|\tilde{k}_i|}{\partial\omega_i^{sc}}\right)^2 u^2} = u\frac{\hat{\omega}_i}{(\omega_i^{sc})^2}\sqrt{\frac{\hat{\omega}_i^2 + (\omega_i^{sc})^2}{\hat{\omega}_i^2 - (\omega_i^{sc})^2}} \tag{14}$$

When ω_i^{sc} becomes lower and lower (and thus $|\tilde{k}_i|$ becomes higher and higher), the value of v decreases and the relative uncertainty $v/|\tilde{k}_i|$ decreases as well. Since this trend cannot be easily derived from Eq. (14), Fig. 3 provides the trend of the uncertainty v, normalised with respect to u, as a function of the $|\tilde{k}_i|$ value for two different cases chosen as examples. All the curves show a decreasing trend of the uncertainty as a function of the $|\tilde{k}_i|$ value, evidencing the benefits provided by the use of an NC.

Therefore, it is strongly suggested to use an additional NC (especially when the initial values of $|k_i|$ are quite low) in order to improve the reliability and the accuracy of the diagnostic method, employing $|\tilde{k}_i|$ in place of $|k_i|$ when calculating s (see Eq. (11)). Another aspect showed by Fig. 3 and worth being mentioned is that the higher the value of ω_i is, the lower the uncertainty associated to the estimation of $|\tilde{k}_i|$ is. Therefore, it is suggested not to consider the very first modes of the structure for the practical application of the method.

4. The effect of environmental and operational conditions

This section is aimed at explaining why the diagnostic method proposed herein is robust to environmental and operational conditions. The two aspects are discussed one by one in the next two subsections.

4.1. The effect of environmental changes

This section aims at discussing some points related to the influence of the most relevant environmental variable, that is the temperature T, on the diagnostic method proposed in this paper. Indeed, the effects of possible changes of the environmental variables are often able to mask the effects of structural changes and this is a well-known problem in structural monitoring (e.g., [51]). Changes of environmental variables are, indeed, able to cause changes of vibration responses and inherent structural properties similar to those generated by a damage. Hence, it is very important to either distinguish them from actual variations caused by structural alterations or find the relationships between environmental variability and trends of the considered damage features [52]. To overcome this issue, advanced data processing can be used, also helping in avoiding masking effects due to operational condition changes. Different recent works are available in the literature, also addressing the complex case of large civil structures (e.g. [52–56]).

Another possibility to overcome this issue is to use a damage feature which is not affected by environmental changes. This strategy, although extremely effective in solving the problem, is the most difficult to apply since, often, the features most sensitive to damage are also the most affected by the environmental and operating variations. This is the case, as an example, of methods relying on the monitoring of eigenfrequencies, which are often biased by the presence of significant temperature shifts. Even though the method proposed here is based as well on the estimate of eigenfrequencies, the $|k_i|$ estimation relies on differential measurements (see Eq. (9)) and this can lead to a different temperature sensitivity with respect to that of eigenfrequencies. Therefore, to estimate the influence of the temperature T on the proposed diagnostic method, its effect on $|k_i|$ must be showed. To quantify the sensitivity of $|k_i|$ to T, it would be necessary to express either ω_i and $\hat{\omega}_i$ (see Eq. (9)) or χ_i and C_{pi} (see Eq. (8)) as functions of physical parameters and study the effect of T on them. However, in both the cases, the results would be related to the specific case considered (e.g., geometry of the structure, materials, boundary conditions) and would not be general. Therefore, due to the exploratory aim of the study, the authors have preferred at first to directly include the effects of the temperature in the numerical simulations presented further in the paper, thus quantifying there the effect of changes of T on the value of $|k_i|$. However, in order to have a rough idea about the effect of the temperature T on the estimated value of $|k_i|$ (or similarly on $|\tilde{k}_i|$), it is possible to calculate the derivative of the expression of $|k_i|^2$ in Eq. (9) with respect to T:

$$\frac{\partial |k_i|^2}{\partial T} = \frac{2\hat{\omega}_i}{\omega_i^2}\left(\frac{\partial \hat{\omega}_i}{\partial T} - \frac{\hat{\omega}_i}{\omega_i}\frac{\partial \omega_i}{\partial T}\right) \tag{15}$$

This equation shows that the effects of the changes of $\hat{\omega}_i$ and ω_i due to changes of T have opposite effects (i.e., opposite signs). This suggests that there is a sort of compensation of the effects that could imply a good level of robustness of the proposed method to the temperature variations. This relevant point, inferred by Eq. (15), will be further confirmed by the numerical analyses presented in Section 6.

It is important to stress that the robustness of the damage feature considered here can make it a good candidate for being given in input to advanced SHM algorithms [54,56]. Indeed, having in input an index that is itself robust to environmental changes can make the performances of advanced methods better and better because they have to compensate only a residual dependence on environmental conditions.

Before concluding this subsection, it is worth evidencing that, thanks to the expected low sensitivity of $|k_i|$ to temperature, it is enough to measure few times $|k_i|$ for determining its natural scatter (due to, e.g., uncertainty in eigenfrequency estimation, noise) before using it for detecting alterations/damages, and no long training is needed.

4.2. The effect of operational conditions

Relying the newly proposed diagnostic approach on the estimation of eigenfrequencies, it is important to have an external source of excitation which allows measuring the structural vibration. If external disturbances acts on the system, they can directly provide the needed excitation, unless they are made from one (or some) mono-harmonic components. Indeed, if the excitation is of random nature, it allows deriving the power spectral density of the structural vibration response and then estimating the eigenfrequencies of the system, without any significant consequence related to a change of the disturbance features. This is true also for other wide-band excitation sources like, e.g., impacts (unless significant non-linearity arises). Conversely, harmonic excitation can generate problems in deriving eigenfrequencies (also when the user provides the needed external excitation) if it has a frequency close to the considered eigenfrequency, regardless its amplitude. In such a case, the proposed approach based on the electro-mechanical coupling can still be applied. Indeed: (i) the method can be applied without including in the damage index the eigenfrequency interested by the harmonic disturbance if other modes provide enough data, or (ii) the method can be applied by shifting the eigenfrequency excited by the harmonic disturbance through the use of an NC in series, if the short-circuit eigenfrequency must be changed, or in parallel, if the open-circuit eigenfrequency must be changed [22]. Therefore, in this case, the NC is used for a different purpose compared to what discussed in Section 3.1. Furthermore, also additional techniques could be used to mitigate the effects of harmonic disturbances on the estimation of eigenfrequency values, as explained in the literature (e.g., [57]).

5. Operative procedure and strengths of the method

This section addresses the procedure to be carried out for applying the diagnostic method presented here. This also gives the possibility to evidence some peculiarities of the approach and its strengths.

The method is based on the monitoring of the trend of the diagnostic index s of Eq. (11) (even calculated on a single mode). This index is based on the estimates of the modal electro-mechanical coupling factors $|k_i|$ (or $|\tilde{k}_i|$ if NCs are used) which in turn are calculated knowing the short- and open-circuit eigenfrequencies of the EMS. Therefore, to evaluate s_p for the pth piezoelectric transducer, two modal analyses with the piezoelectric transducer in short-circuit and, then, in open-circuit are required, allowing for identifying the eigenfrequencies of the modes involved in the s_p calculation. Once the values of ω_i (or ω_i^{sc} if an NC in series is shunted to the piezoelectric transducer) and $\hat{\omega}_i$ (or ω_i^{oc} if an NC in parallel is used) have been estimated with the modal extractions, the values of $|k_i|$ (or $|\tilde{k}_i|$) can be calculated (see Eqs. (9), (12) and (13)) for all the considered modes and, then, the index s_p is calculated (see Eq. (11)). In case more than one piezoelectric transducer is available, the above procedure can be performed for all of them, working with one transducer at a time, and keeping all the others in the same reference condition (i.e., either short- or open-circuited).

Deviations of s from the null value can indicate the presence of a structural alteration. However, since a single s value significantly different from 0 can be caused, as examples, by a bias on the identified eigenfrequency values, or by noise, or by other disturbance effects, the method is based on the monitoring of the s trend rather than on a single occasional observation. Indeed, it is possible to calculate s many times allowing for the identification of any persistent change of s (i.e. occurring for more than one acquisition), which can be thus actually attributed to a change of the structure. Moreover, different types of distances can be used for automating this check (e.g., [58,59]).

From the practical point of view, since the estimate of $|k_i|$ is based only on eigenfrequency identifications (in both short- and open-circuit conditions), the modal extraction can be carried out either exciting the structure or exploiting just the environmental excitation, thus using operational modal analysis [60]. Changes of operational conditions, which are often a source of uncertainty in alteration detection [61], are not expected to affect the method reliability because the approach is based only on eigenfrequency estimation (just cases where significant non-linearity arises can affect the method). The only requirement is to have a remote switch able to change the piezoelectric transducer configuration (i.e., either open- or short-circuit) and a device able to measure vibrations (e.g., a low cost accelerometer or even another piezoelectric transducer in case more than one is available on the structure). It is worth underling that the number of vibration sensors depends on the number of modes involved in the calculation of s. Even a single sensor could be enough if sensitive to all the required modes.

The description of this diagnostic procedure allows evidencing some strengths of the approach. The simple idea behind the method evidences the possibility of using already available piezoelectric transducers and an index that can be calculated relying on the estimation of eigenfrequencies, which can be performed with well-established instruments and procedures. These features make the proposed method easy to apply and interpret, and, overall, allows having the chance to monitor a system/structure even when no monitoring system is already present. Furthermore, since the piezoelectric transducers are a mature and wide-spread technology, the diagnostic method results less expensive compared to other commonly employed methods (e.g., use of dense sensor meshes, fibre optic devices, etc.). This is also due to the fact that a single or a few measurement points are required, without any need of synchronous acquisition, and, thus, a single measurement channel is needed on the analog-to-digital acquisition board even when more than one piezoelectric transducer is used for the diagnostic approach. Another relevant aspect which contributes in making the method not expensive and easy to apply is the possibility of working in the low frequency range. Despite the technique does not prevent the inclusion of high frequency modes in the evaluation of the index s, their use can be limited by the very low electro-mechanical coupling usually faced at high frequency. Although it could seem a limitation for the proposed approach, this aspect is advantageous both because this does not imply the use of dedicated and tailored electronic devices and because it allows employing possible already available devices and transducers which, in usual applications such as vibration control and energy harvesting, mainly work in the low-frequency range.

It is worth evidencing that this peculiarity of the proposed damage feature contributes differentiating the presented SHM approach by the EMI techniques. EMI techniques, indeed, mostly work at high frequency (even if EMI can be used also at low frequency in some specific cases [20]) and are not directly related to system eigenfrequencies [62,63] since they focus on the capability of waves to propagate through the structure. They require a size of the piezoelectric patch small enough to detect small damages and, often, are sensitive to temperature variations [64] which cause system changes and force to adopt calibration procedures [65]. Conversely, the method discussed here considers an index based on the efficiency of the electro-mechanical conversion of energy (measured by the quantity $|k_i|$) in correspondence of the system resonances and thus its optimal working range is in the low-frequency region (i.e., up to a few thousand Hertz at most). Furthermore, the physical principle behind the considered damage feature does not link the size of the damage to that of the piezoelectric transducer. This is because the index $|k_i|$ depends on the change of the mode shape at the transducer boundaries caused by the alteration, thus allowing for a small alteration being detected by much larger transducers, as will be shown in Section 7.1. This does not mean that the size of the transducer has no consequences on the capability to detect the alteration in the proposed method: a change of the transducer size involves a change of the $|k_i|$ values [25,27,66] for the different modes, making some modes more sensitive than others. Finally, the proposed approach, unlike EMI techniques, shows a good robustness with respect to temperature variations. This is mainly due to the fact that the estimate of the modal electro-mechanical coupling factor relies on differential measurements of eigenfrequencies, unlike EMI techniques which are based on a single spectral measurement.

Finally, this diagnostic method is able to work with the structure under operating condition. Of course, when the method exploits already available piezoelectric transducers, its applicability is limited by the possibility of switching off the other systems employing the transducers (or, at least, of switching to SHM functions a single transducer at a time), and by the possibility of exciting the system while working in case the environmental excitation is not of sufficient extent or is in a limited frequency range. Finally, it is worth underling that the capability of the approach to be robust to environmental and operational conditions suggests that the use of the

Table 1
Nominal data used for the simulations at two different temperatures. Here, ϵ_0 is the free space permittivity and it is equal to 8.854×10^{-12} F/m.

	$T = T_0 = 293.15$ K	$T = 253.15$ K
Aluminium		
Young's modulus [GPa]	71.00	72.34
Poisson's coefficient	0.3	0.3
linear thermal expansion coefficient [m/(m K)]	2.4×10^{-5}	2.4×10^{-5}
PIC151		
Poisson's coefficient	0.34	0.34
elastic compliance S_{11}, S_{22} [m^2/N]	1.50×10^{-11}	1.55×10^{-11}
elastic compliance S_{33} [m^2/N]	1.90×10^{-11}	1.96×10^{-11}
dielectric constant [F/m]	$2400\epsilon_0$	$2252\epsilon_0$
piezoelectric strain constant d_{31} [C/N]	-2.10×10^{-10}	-2.07×10^{-10}
piezoelectric strain constant d_{32} [C/N]	-2.10×10^{-10}	-2.07×10^{-10}
piezoelectric strain constant d_{33} [C/N]	5.0×10^{-10}	4.9×10^{-10}
piezoelectric strain constant d_{15} [C/N]	5.8×10^{-10}	5.0×10^{-10}
material coupling factor $\hat{k}_{31}$	0.38	0.37

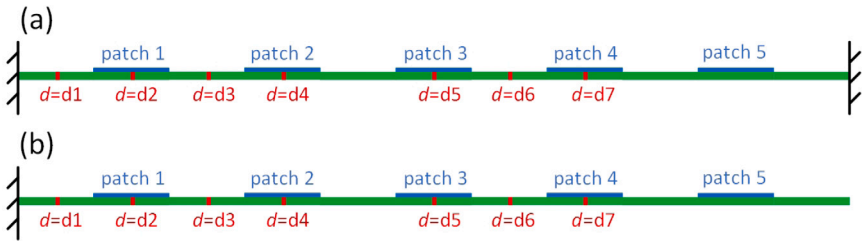

Fig. 4. The two beams used for the numerical investigations: clamped–clamped configuration (a) and cantilever configuration (b). The length of the patches and of the beam portions without the patches is equal to 70 mm (i.e., total length of the beams equal to 770 mm); thickness equal to 1 mm for the beams and 0.5 mm for the piezoelectric patches (the beams and the patches have the same width). The letter d indicates the locations of the structural alterations in the simulations, that are always placed in the middle of portions either with or without a piezoelectric patch.

index s as an additional input to advanced monitoring algorithms can result in an improvement of their performances because the compensation of the environmental and operational conditions becomes easier.

In a future perspective, when embedded and smart structures (e.g., [67]) will become more and more common and inexpensive, also thanks to the additive manufacturing techniques, this easy-to-apply diagnostic feature and its promising robustness to changes of environmental and working conditions, as well as its ability to work even when the system is operational, can give self-monitoring capabilities to each structure by simply exploiting the coupling properties offered by these systems.

6. Numerical analyses

This section is aimed at showing the feasibility of the proposed approach and at evidencing the aspects which must be deepened for making the approach mature for real applications. To this purpose, the results of finite element (FE) simulations are used at first to evaluate the effectiveness and the sensitivity to structural alterations of the proposed approach.

The structures chosen for the simulations are light, thin and with a simple layout. The choice of light and thin structures is related to the fact that these are the usual structures where piezoelectric patches are employed for vibration control, energy harvesting, etc., thanks to the possibility of having significant values of $|k_i|$. However, in case stack elements are used, the size and mass of the structure could be increased thanks to the higher forces generated by stacks compared to patches (see, as an example, Section 7.2). Furthermore, the choice for a simple layout is related to the goal of the study, which is to evaluate the feasibility of the method and a complicated layout would not add anything significant for this purpose (also causing an increase of the computational burden).

The structures considered in the simulations were beams (this does not imply any loss of generality of the results, which are expected to be similar for bi-dimensional structures) with different boundary conditions. The piezoelectric patches simulated were chosen among those already available on the market (typical size was considered and the material was chosen among the commercial ones to obtain high values of $|k_i|$) and different patches were placed on the beams in given positions, without any initial check on the $|k_i|$ values of the first fifteen bending modes of the beam. Therefore, the patches were not optimised in terms of geometry and position on the beam. The choice of considering generic patches in generic positions is aimed at checking whether the proposed method can actually be feasible in real applications, where (i) space constraints could limit the possible locations for placing piezoelectric elements, (ii) piezoelectric transducers available for other purposes could be exploited, thus having fixed position and geometry which could not result optimal for the structural monitoring. On the one hand, this situation is of course not realistic and not favourable since, even in case of using an already existing set of transducers whose task is, e.g., vibration control, their $|k_i|$ values

would be optimised at least on the modes to be controlled. On the other hand, this layout of the patches allows testing the method in the worst condition. It is, however, important to evidence that, according to the literature (e.g., [25]), using a good material available from manufacturers (e.g., PIC151) and a thickness of the piezoelectric patch equal to, say, 20%–50% of that of a mono- or bi-dimensional vibrating structure, it is possible to obtain $|k_{i,p}|$ values close to 0.1 for different modes, which is a value easily detectable through experimental estimation of short- and open-circuit eigenfrequencies.

As mentioned, in all the simulations and experiments of this paper, the piezoelectric elements were not optimised in terms of size and position and the authors also decided to work sometimes with modes with small initial values for $|k_{i,p}|$. These choices come from the will to show that, even in such cases, it is still possible to detect alterations with good reliability, thanks to the adoption of NCs to pass from $|k_{i,p}|$ values to $|\tilde{k}_{i,p}|$ values.

Two test-case beams were considered: a clamped–clamped beam and a cantilever beam. They were made from either aluminium or steel. Here, for the sake of conciseness, results are shown only for aluminium, with a main focus on the clamped–clamped beam. However, there are no significant differences in the results of the analyses for the different cases that were considered. Five piezoelectric patches (material PIC151) were simulated as bonded on the beam (assuming a tie constraint). The beams are represented in Fig. 4 and Table 1 reports some material parameters (assumed at environmental temperature $T = T_0 = 293.15$ K).

The structural alteration was simulated in different locations (see the areas denoted as $d = \mathrm{d}1, \ldots, \mathrm{d}7$ in Fig. 4), and it was applied in a single location at a time, whereby there are no simulations where a structural alteration is present in more than one location. The structural alteration was simulated by decreasing the value of the Young's modulus of a considered section of the beam of a given percentage value D (i.e., $D = 30$, 50, 70 and 90%), as done in many referred papers (e.g., [44]). The cross-area of the structure affected by the alteration was equal to the cross-section of the beam and its length was set to 5 mm, corresponding to approximately 0.65% of the clamped–clamped beam length. However, it is underlined that any type of structural modification involving a significant mode shape change can be considered as well (see previously in the paper).

The FE model was developed in Abaqus employing solid elements with 20 nodes; the size of the elements along the beam length was approximately equal to 2 mm for both the beam and the piezoelectric transducers and it was set after a convergence analysis (the ratio 2/770 between the length of the single finite element and the beam length allows for properly describing the first fifteen bending modes considered in the simulations). The $|k_{i,p}|$ and $|k_{i,p,\mathrm{a}}|$ values (see Eq. (10)) for these first fifteen bending modes were calculated for each patch according to Eq. (9), thus estimating ω_i and $\hat{\omega}_i$. When the short- and open-circuit eigenfrequencies were calculated with the FE model for a given patch, all the other patches were short-circuited. Therefore, according to Eq. (9), $|k_{i,\mathrm{p}}|$ was calculated as (the same applies to $|k_{i,\mathrm{p,a}}|$):

$$|k_{i,\mathrm{p}}| = \sqrt{\frac{\hat{\omega}_{i,p}^2 - \omega_{i,\mathrm{all}}^2}{\omega_{i,\mathrm{all}}^2}} \tag{16}$$

where $\omega_{i,\mathrm{all}}$ is the ith eigenfrequencies when all the patches are short-circuited and $\hat{\omega}_{i,p}$ is the ith eigenfrequencies when the pth patch is open-circuited and all the other patches are short-circuited.

The equipotential condition of each of the electrodes of the piezoelectric elements was assured by applying a coupling constraint to all electric potential degrees of freedom that are part of a continuous electrode, whereby the resulting electrode potential is represented in a so-called master node [23]. The short-circuit condition was simulated by wiring the two electrodes of the considered piezoelectric element imposing a coupling constraint to the corresponding two master nodes. Obviously, for open-circuit condition, this additional constraint was not added and only one electrode was grounded.

6.1. Results

This subsection shows some results obtained by means of the mentioned test-case structures. Section 2.2 showed that the percentage variation of $|k_i|$, expressed by the index $\Delta_{i,p}$ (see Eq. (10)), suffers from some drawbacks and is not suggested as diagnostic index due to its sensitivity to possible uncertainties on the estimated parameters. However, some analyses related to the behaviour of $\Delta_{i,p}$ are presented here to evidence the effect of a structural alteration on the modal electro-mechanical coupling factor associated to each of the different modes separately. These effects are, instead, hidden in the index s where the contributions of all the considered modes are summed. To this purpose, Fig. 5 shows the values of $\Delta_{i,p}$ (i.e., the percentage change of the $|k_i|$ value for the pth patch due to an alteration, see Eq. (10)) for the clamped–clamped beam and for some bending modes chosen as examples, when the alteration is close to the piezoelectric patch considered for calculating the $\Delta_{i,p}$ values. As an example, Fig. 5a shows the $\Delta_{i,p}$ values for patch 1 and alteration location d1 (i.e., when the patch and the alteration are close each other, see Fig. 4) when $D = 30\%$, while Fig. 5b shows the same data when $D = 50, 70, 90\%$. The different levels of D have been shown in different plots because, otherwise, the effect of $D = 30\%$ would have been hidden due to the full-scale of the plot. It is clear that, even with the smallest value of D, some modes show significant changes of the $\Delta_{i,p}$ value (e.g., modes 1, 3, 11, 14 and 15). Nevertheless, there are also $|k_i|$ values not affected by the alteration in the chosen location (e.g., for mode 12). This can occur because either the alteration does not affect the considered mode shape at all or the considered piezoelectric transducer boundaries are in positions where the mode shape is not changed. Furthermore, Fig. 5b shows that the value of $\Delta_{i,p}$ usually increases with the severity of the alteration (i.e., with increasing values of D). A similar behaviour occurs also for patch 4 and an alteration in location d6 (see Figs. 5c and d).

When, instead, the alteration is far from the patch considered, the number of modes showing significant changes of the $\Delta_{i,p}$ value decreases (see Figs. 4 and 6). As an example, for $D = 50\%$, different modes show values of $\Delta_{i,p}$ either close to or higher than 10% for patches close to the alteration (see Figs. 5b and d), while this does not occur for patches far from the alteration (see Figs. 6b

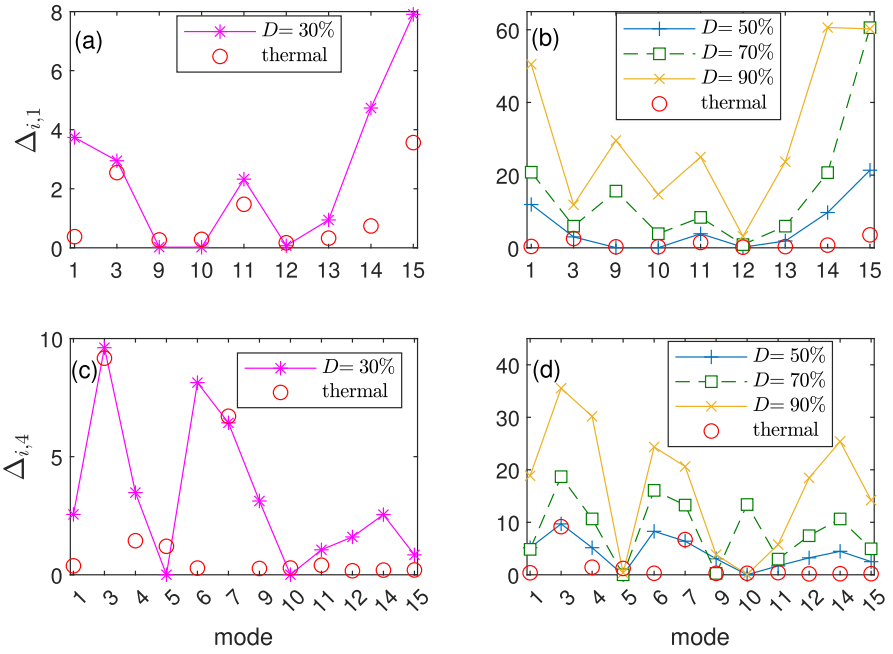

Fig. 5. $\Delta_{i,p}$ values for patch 1 and alteration in location d1 for D = 30% (a) and 50, 70, 90% (b), and for patch 4 and alteration in location d6 for D = 30% (c) and 50, 70, 90% (d) for the clamped–clamped beam. The $\Delta_{i,p}$ values caused by a thermal shift of −40 K for the unaltered beam are also plotted as circles.

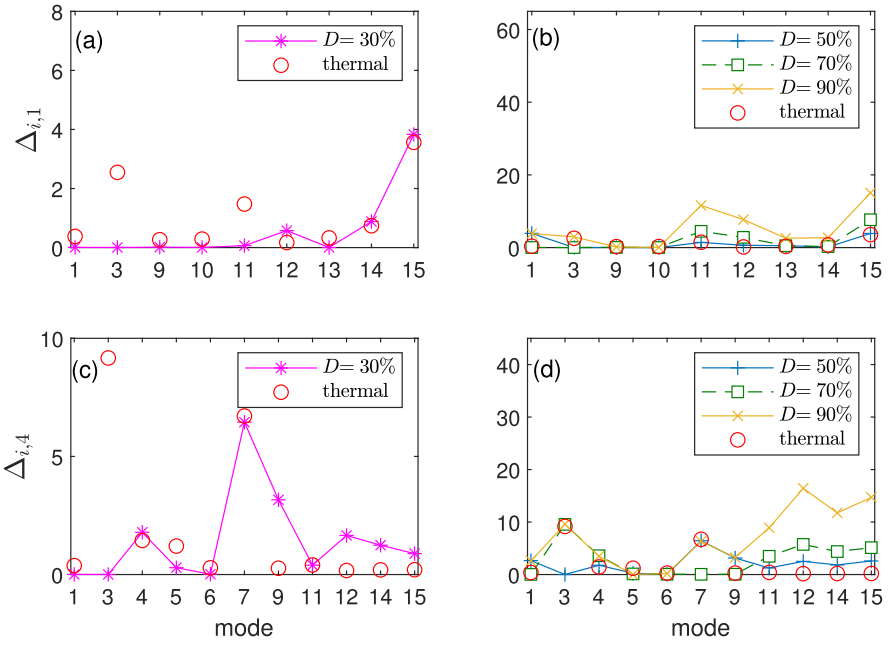

Fig. 6. $\Delta_{i,p}$ values for patch 1 and alteration in location d7 for D = 30% (a) and 50, 70, 90% (b), and for patch 4 and alteration in location d4 for D = 30% (c) and 50, 70, 90% (d) for the clamped–clamped beam. The $\Delta_{i,p}$ values caused by a thermal shift of −40 K for the unaltered beam are also plotted.

and d). Moreover, when the considered patches are far from the alteration, also the greatest values of $\Delta_{i,p}$ decrease compared to the case in which the alteration is close to the considered patch.

As mentioned in Section 4.1, it is essential to investigate the effect of the environmental changes and verify that the changes of $|k_i|$ due to a structural alteration are not masked by its changes related to the environmental variables. To this purpose, a temperature change of −40 K (i.e., from $T = T_0$ = 293.15 K to T = 253.15 K) was applied to the non-altered beams of Fig. 4 and the material and geometrical features were changed accordingly. Table 1 gathers the data of the materials (aluminium and PIC151) for the two

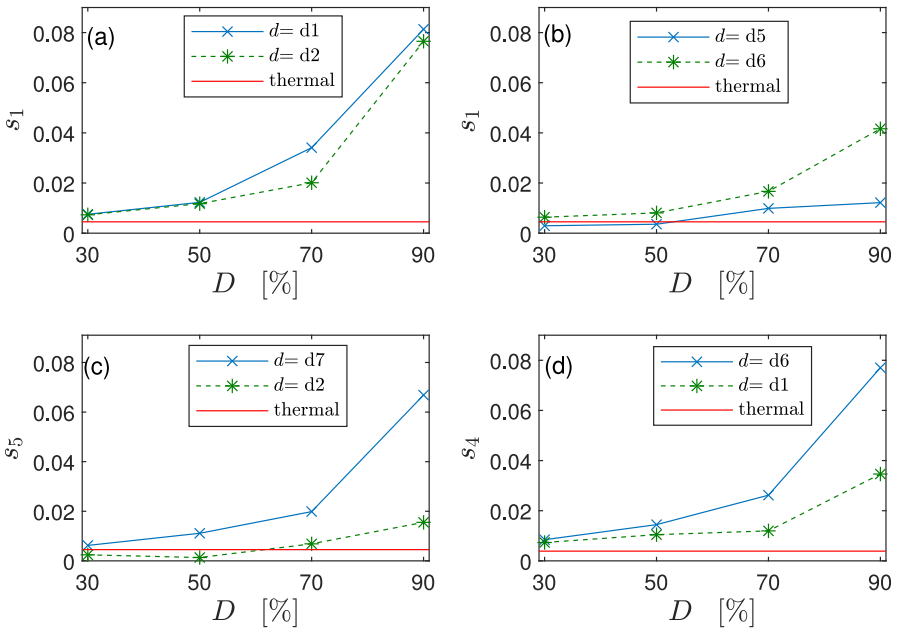

Fig. 7. s values for patch 1 in the clamped–clamped beam in case of either close (a) or far (b) damage. s values for patch 5 in the clamped–clamped beam in case of both close and far damage (c). s values for patch 4 in the cantilever beam in case of both close and far damage (d). The s values caused by a thermal shift of −40 K for the unaltered beams are also plotted. All the s values are calculated considering the bending modes between the fifth and the fifteenth.

different temperatures. The data for the material PIC151 were extracted from the data-sheet available from the manufacturer of the piezoelectric patches [68]. In the case of the clamped–clamped beam, the change of temperature also led to the appearance of a tensile axial load due to the presence of two constraints at both ends of the beam. Figs. 5 and 6 show the $\Delta_{i,p}$ values due to the temperature change with circles for the non-altered clamped–clamped beam. Most of the times, the values of $\Delta_{i,p}$ due to the simulated alterations are higher than those generated by the temperature change, even for the lowest value of D, thus suggesting a good robustness to temperature of the proposed approach (see also further in this section). As examples, consider the $\Delta_{i,p}$ values for modes 1 and 15 in Figs. 5a and b, and for modes 4 and 6 in Figs. 5c and d. The few cases where the $\Delta_{i,p}$ values generated by the thermal shift become significant (e.g., higher than 4%, see modes 3 and 7 in Fig. 5c as examples) are usually related to modes with a small initial value of $|k_{i,p}|$. Therefore, their effect in the s index will be small/negligible, further proving the advantages of using index s in place of $\Delta_{i,p}$.

The analyses of the $\Delta_{i,p}$ values evidenced that a certain alteration either can or cannot affect a given mode in a given location and, thus, either can or cannot affect the corresponding $|k_i|$ value. Although this would suggest the need of knowing the modes affected by a possible damage (thus, making the application of the method cumbersome), the problem is overcome by the use of the index s (see Eq. (11)). Indeed, the damage index s is calculated on a given amount of modes and, thus, allows not to analyse in advance which modes are affected by a given damage in given locations. Fig. 7 shows the value of s, calculated for the bending modes between the fifth and the fifteenth. The very first bending modes were discarded in this case to simulate a real application where they would be neglected due to the high uncertainty associated to their $|k_i|$ estimation (see Section 3.2). Indeed, all the modes between the first and the fifteenth showed comparable values of $|k_i|$ and, looking at Fig. 3, the $|k_{i,p}|$ estimates for low-frequency modes would have been affected by a larger uncertainty compared to those at higher frequency. Figs. 7a, b and c show the trend of s for the clamped–clamped beam as a function of the value of D for different patches and different locations of the damage (see Fig. 4). The value of s has an increasing trend as a function of the damage severity. Furthermore, when the piezoelectric patch is close to the damage, the values of s tend to be higher than when the patch is farther from the damage (compare plot (a) with plot (b) in Fig. 7, and also the lines related to different d values in plot (c)). These features of the s index confirm its reliability for the detection of the structural alteration. A similar outcome is obtained also for the cantilever beam (see Fig. 7d). Furthermore, in these plots, the s value caused by the thermal decrease of 40 K for the undamaged beam is represented with a horizontal solid line. When the damage and the patch are close, the thermal effect is usually not able to generate s values higher than those caused by the damage, also for the lowest D value. When, instead, the damage moves away from the transducer location, the s value is still able to identify the alteration but this occurs for damage entities more severe than in the previous case (e.g., the damage can be identified only when $D = 70\%$ and 90% for $d =$ d6 in Fig. 7b and $d =$ d2 in Fig. 7c).

It is interesting to evidence that the changes of the short-circuit eigenfrequencies generated by the temperature decrease were always higher than those caused at environmental temperature T_0 by the largest decrease of the Young's modulus (i.e., $D = 90\%$) for all the considered bending modes of the two beams. The same occurred for the open-circuit eigenfrequencies. Therefore, although it is not possible to monitor the eigenfrequencies in order to detect a structural alteration because its effects are masked by the effects

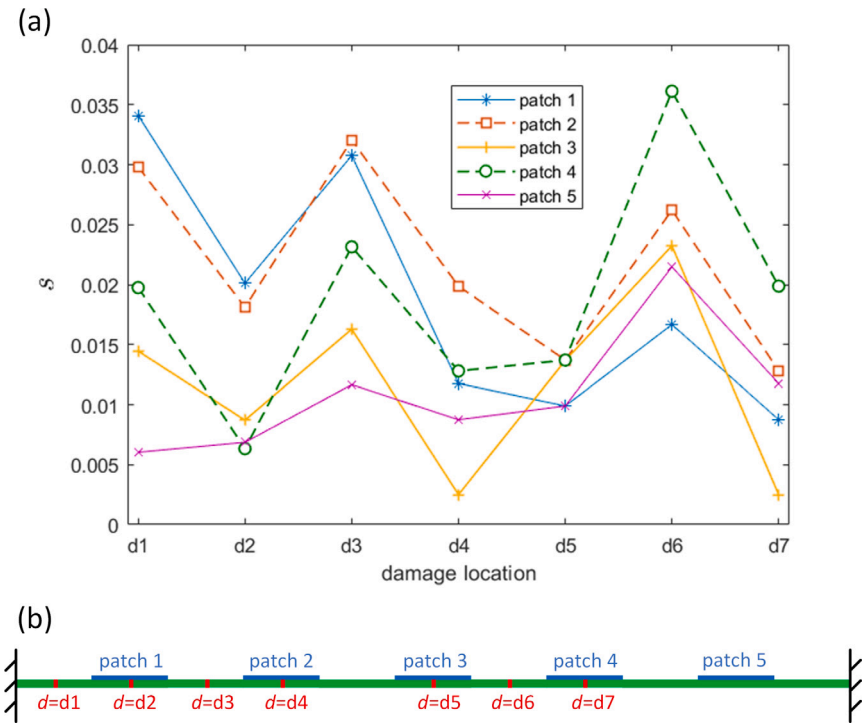

Fig. 8. s values (calculated over the bending modes between the fifth and the fifteenth) for the different patches of the clamped–clamped beam as functions of the damage location, with D = 70% (a) and the schematic of the beam (equal to Fig. 4a) for facilitating the readability of the figure (b).

of the environmental conditions, it is possible to use them to estimate the electro-mechanical coupling and calculate s. The index s is, indeed, robust to temperature changes and its value due to an alteration is usually higher than that produced by a temperature shift, even when the smallest value of D is considered. Fig. 7 shows that values of s due to an alteration are larger than those related to the temperature change, and the only exceptions may occur in cases the piezoelectric patch is far from the alteration and thus less sensitive to its presence.

Even if the capability of the index s to provide an indication about the location of the damage is not deepened here, it is worth showing that the index s can be fruitfully employed to obtain an indication about the alteration location. Fig. 8 shows the value of s (calculated for the bending modes between the fifth and the fifteenth) for the different piezoelectric patches and the different alteration locations, for the clamped–clamped beam and D = 70% (see Fig. 8b). At all the damage locations, the patch closest to the damage shows the largest value of s and this allows for an indication of the alteration location. As an example, for damage location d = d1 (see Fig. 8b), the patch providing the largest value of s is the first one, that is the closest to the alteration. The only alteration location where a doubt could arise is related to d = d5. Here, three patches are showing similar values (i.e., patches 2, 3 and 4). However, three considerations are worth being provided for this case:

1. patch 3 is exactly in the middle of the beam and, thus, is sensitive only to odd modes (i.e., those without a node in the middle of the beam). This limits the value of s associated to this patch and, indeed, this s value is always not high, even for the other damage locations;
2. the damage is exactly in the middle of the beam and is thus able to change the $|k_i|$ values only for odd modes. Indeed, all the patches show a low value of s for the damage in this location;
3. the patches showing the largest (and similar) values of s are the second, the third and the fourth, that are the piezoelectric elements close to the alteration (i.e., the damage is exactly in the middle between patches 2 and 4, see Fig. 8b). Therefore, even in this case, the index s is able to provide a reliable indication of the damage location, even if the spatial resolution of the information worsens.

A further figure is presented here to prove the possibility of using the index s to obtain indications about the alteration location. Figs. 9a and b show a map of the values of s for D equal to 50 and 70%, respectively. For all the damage locations, the index s has been normalised (the normalised value is referred to as $\bar{s}$) such that it is equal to 1 for the patch having the highest s value for the considered damage location. Therefore, for each damage location (i.e., for each column of the plot), the value of $\bar{s}$ associated to each patch is shown in gray scale, where black is 0 and white is 1. It is evident that the area for which $\bar{s}$ is close or equal to 1 (light area) moves from the patches in the left part of the beam towards those on the right side as soon as the damage location moves in the same direction (see Fig. 4). The light area moves, indeed, following the solid red line and the red circles indicate the positions

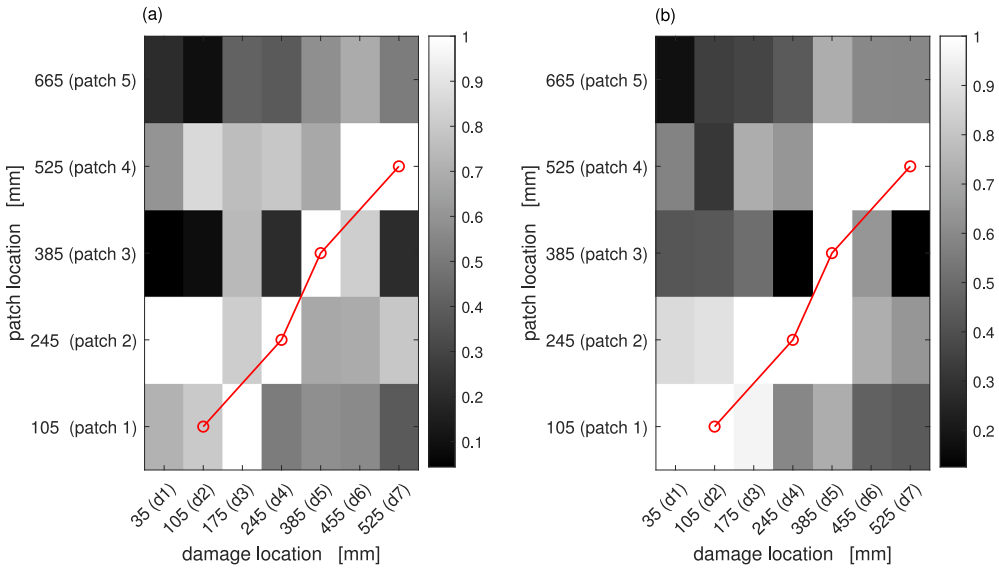

Fig. 9. $\bar{s}$ values (calculated over the bending modes between the fifth and the fifteenth) for the different patches of the clamped–clamped beam as functions of the damage location for $D = 50\%$ (a) and $D = 70\%$ (b). The labels on the figure axes refer to the centre of the patches and the damage sections. The solid red line indicates the spatial correspondence between the horizontal and vertical figure axes (see the text for more details).

where the centre of a given patch is in correspondence of a damage, and vice versa. This behaviour is more and more evident when the value of D increases. These two figures further prove the reliability of s in providing information about the alteration location. Therefore, when a given transducer is close enough to alteration to detect it through the index s, it is then also able to add pieces of information useful for assessing the alteration location. However, the index s must not be considered as able to provide the exact location of the structural alteration because its value depends on the number of modes which is possible to take into account in the sum of Eq. (11). When the number of modes decreases, also the capability of s in providing the exact location of the damage decreases. An example of this behaviour is given by s_3 (i.e., the value of s for the third patch) in the case of the clamped–clamped beam (see Fig. 8): its value is always lower than the values calculated for the other patches since it always works only on the odd modes because of its geometrical position on the structure (i.e., in the middle of the beam). Therefore, the index s must be considered as capable of giving only an indication of which areas must be investigated at first. Figs. 9a and b properly explain how to use the index s to get indications about the damage location: the area that must be considered at first is the lightest one (i.e., the area related to the patches showing the largest s values).

Before introducing in Section 7 the results of the experimental activity carried out to validate the outcomes of this section, it is worth spending few words about the number of modes used to calculate s. In the analyses shown in this section, eleven eigenfrequencies were considered, from the fifth to the fifteenth. This choice is related to the need of evidencing the method potentialities and the index characteristics. It, indeed, allowed evidencing the differences in the index s when few or all the modes can be used (e.g., consider the case of s_3 in Fig. 8) as well as the possibility of increasing the method sensitivity by considering several modes. However, despite some slender bi-dimensional structures would allow the identification of such a high number of modes, eleven seems a high number, especially if the case of the eigenfrequency identification with operational modal analysis is considered or in case of either complex or damped structures. Despite an analysis about the method sensitivity to the number of modes used to evaluate s has not been carried out here, because beyond the scope of this feasibility study, the experiments evidence that the proposed approach satisfactorily works even when few modes can be used for the considered structure. Therefore, it is possible to state that the method works regardless the number of eigenfrequencies used but its sensitivity and reliability can be improved by increasing it.

7. Experiments

This section presents two different test types aimed at showing the feasibility of the method proposed here and its effectiveness and strengths. Section 7.1 discusses different tests with a cantilever beam where the alteration is simulated by adding a small mass in order to evidence the different features of the approach such as, e.g., the good robustness to temperature changes. Then, Section 7.2 will discuss a case where a more complex structure (i.e., a truss) is considered and a real damage is intentionally introduced in the system.

7.1. Tests with a cantilever beam

The set-up used was composed by an aluminium cantilever beam with five piezoelectric patches (material PIC151; see the caption of Fig. 10 for size and locations) bonded on one of its sides. The beam was connected to an electro-dynamic shaker at the clamped

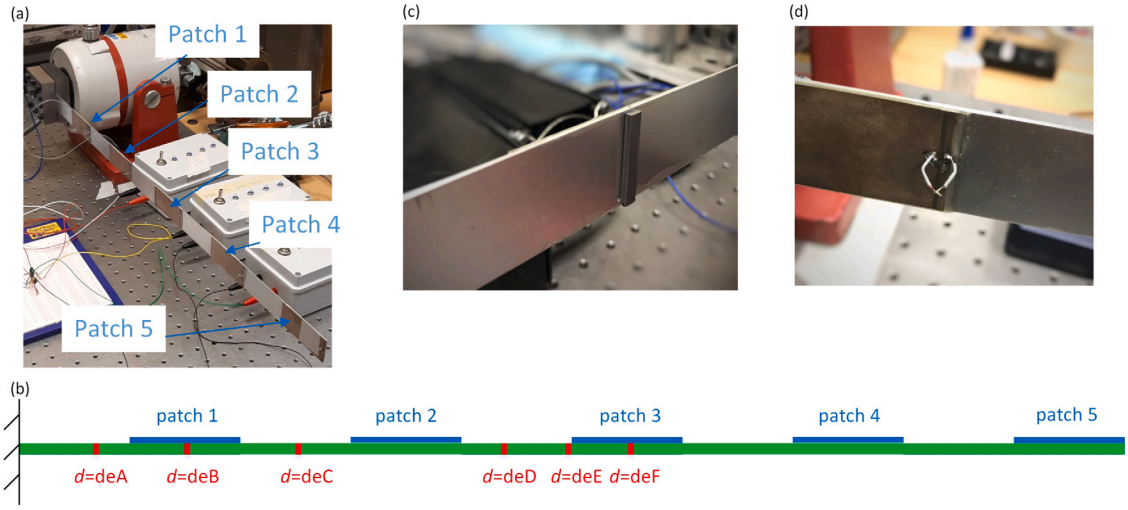

Fig. 10. The set-up (a), its geometrical configuration where the length of the parts either with or without the patch is equal to 70 mm, the thickness of the beam is equal to 1 mm and that of the patches is 0.5 mm (see more details in Table 2) (b), a picture of the brick bonded to the beam (c) and the short wires used to obtain the short-circuit configuration (d).

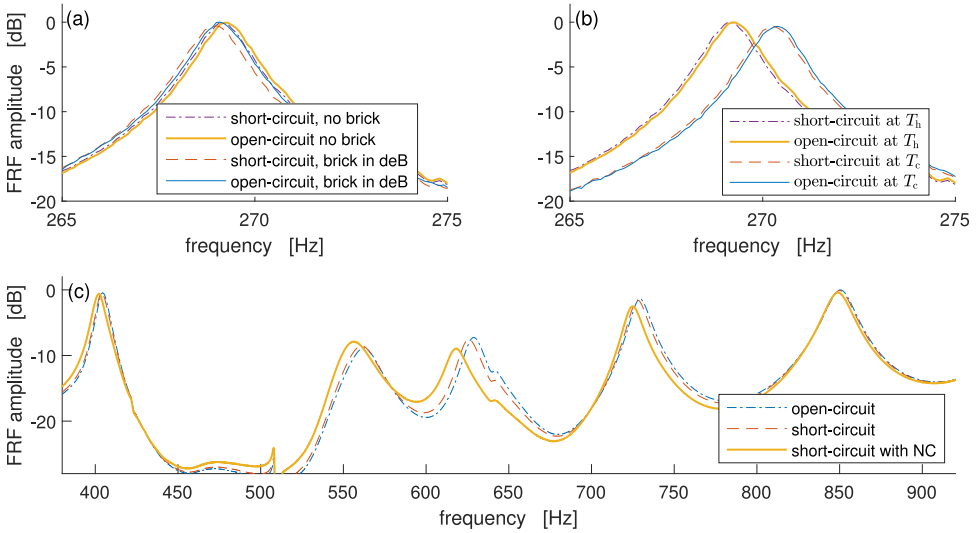

Fig. 11. Amplitude of experimental FRFs between the acceleration provided at the constraint and the response of the beam tip with patch 1 in different configurations (with all the other patches short-circuited): FRFs at T_h with and without the brick zoomed on a single mode (a), FRFs at T_h and T_c without the brick zoomed on a single mode (b), FRFs with and without the NC in series and without the brick (c). In all the plots, the highest peak has been scaled to 0 dB.

Table 2
Locations d of the brick (see Fig. 10b).

Brick location identifier	Distance between the beam constraint and the centre of the brick along the longitudinal axis of the beam [mm]
deA	47.5
deB	105.0
deC	175.0
deD	302.5
deE	347.5
deF	385.0

end. The shaker was used to provide random excitation to the system in the desired frequency range (more details will be given when discussing the test results). The response of the beam was collected by means of either a laser velocimeter (Ometron VH300+ Laser Doppler Vibrometer, Type 8329) or an accelerometer (PCB Piezotronics, type 333B30) both measuring close to the tip. The estimator H_1 [69] was used to calculate the frequency response functions (FRF) of the beam, then employed for modal extraction with the Least Squares Complex Frequency domain method [70]. These FRFs were calculated between an accelerometer (type 333B30) measuring the motion imposed by the shaker to the clamped end and the accelerometer/vibrometer measuring at the beam tip. The set-up is shown in Fig. 10a, while Fig. 10b describes the geometrical layout of the system. The whole set-up was placed in a room with controlled temperature. This allowed for carrying out the tests at two different temperatures: $T_h \simeq 300.15$ K and $T_c \simeq 288.15$ K.

The alterations were not produced by damaging the beam because this would have required many different beams with many different piezoelectric patches. Therefore, the structural alterations were obtained by adding a small brick glued to the beam in different positions along its length (see Fig. 10b and Table 2). This choice allowed both working on the same structure, just changing the system alteration, and reducing the cost of the set-up (i.e., no need of several beams and transducers). As for the first aspect, avoiding the use of different beams allowed reducing the possible uncertainties related to different beams, constraints, transducer positions, material, etc. In this way, it was possible to ascribe any change of the damage feature to the controlled parameters (either T or the alteration) and to validate the approach behaviour. However, to take into account also more realistic damage conditions, the experiments of Section 7.2 were carried out.

A picture of the brick used to simulate the alteration and bonded to the beam is provided in Fig. 10c. The brick was designed so that changes of the $|k_i|$ and $\Delta_{i,p}$ values close to those obtained for $D = 30, 50$ and 70% in the simulations of Section 6 were achieved. This was considered important to test the feasibility of the measurement of $|k_i|$. As an example, in Section 7.1.1, tests will be shown where some modes find their $\Delta_{i,p}$ values equal to approximately 10%. This value is found also, as an example, in the results related to the simulations of Fig. 5.

The short- and open-circuit tests were made possible by adding small wires to the patches, as evidenced in Fig. 10d. During the tests, one patch at time was considered, while the other patches were kept short-circuited. Fig. 11a shows some FRFs, zoomed on a given bending mode, between the accelerometer measuring the input provided by the shaker and the vibration structural response, with the piezoelectric patch 1 in either short- or open-circuit at temperature T_h. This plot also evidences the slight shift of the eigenfrequencies due to the brick located in position deB (see Fig. 10b). Furthermore, Fig. 11b shows the FRF for the same mode comparing the beam response without the brick but at two different temperature values. It is evident that the eigenfrequency shift due to the temperature change is significant and larger than that caused by the brick (compare plots (a) and (b)).

In the following subsections, two sets of tests will be analysed. The first tests presented are aimed at showing three main aspects: (i) the sensitivity of the $|k_i|$ values, and thus of the method proposed, to structural alterations and the benefits provided by the use of an NC, (ii) the repeatability of the estimation of $|k_i|$ through Eq. (9) and (iii) the low influence of the temperature on the value of $|k_i|$. The number of repetitions carried out in the different tests are limited and aimed at just showing the method feasibility and highlighting its properties. The promising results shown in Section 7.1.1 will evidence that it is worth carrying out future in-depth statistical analyses. The second set of tests is instead aimed at showing that the proposed method based on the index s can be used to both evidence the presence of a damage and obtain information about its location. These two types of tests are described and discussed in Sections 7.1.1 and 7.1.2, respectively. For the sake of conciseness, mainly the tests associated to the first and third patches are reported.

7.1.1. Sensitivity to alterations, repeatability and temperature effects

In this case, the broadband disturbance acting on the structure was provided in a frequency range between approximately 90 and 1250 Hz.

Fig. 12 is related to the first patch (see Fig. 10b) and shows, for some of the modes identified (indicated in the figure through nominal values of the corresponding eigenfrequencies), the estimated $|k_i|$ values. Each $|k_i|$ value was estimated at two different temperatures T_h and T_c (blue circles and asterisks, respectively) and each test was repeated two times. The results coming from the repetitions of the same test are well superimposed, evidencing a good repeatability of the results and confirming the low influence of the temperature (see Sections 4.1 and 6.1). The results of a fifth test are also reported in the same figure (evidenced with red plus symbols), where the brick was added in position deB (see Fig. 10b and Table 2). It is evident that, for some modes, a clear shift of the $|k_i|$ value occurred, highlighting that the brick effect on $|k_i|$ is more evident than that of the temperature. Since the presence of the brick causes changes of the $|k_i|$ values close to those obtained in the FE simulations presented previously in the manuscript, also a decrease of the beam Young's modulus (even for low D values) is expected to be more evident than the temperature effects. Fig. 12 also evidences that the effect of an alteration is different for the various considered modes (e.g., mode at about 602 Hz compared to that at approximately 1082 Hz).

To deepen this aspect, further tests were carried out to the aim of showing the effect of the different positions of the brick on the value of $|k_i|$ of different modes. In these tests, the brick was placed in positions deB, deC or deF (see Fig. 10b). For each location of the brick, four test repetitions were carried out in order to check again the repeatability: from test 1 to test 4 for location deB, from test 5 to test 8 for location deC and from test 9 to test 12 for location deF in Figs. 13 to 15. These tests were performed at $T = T_h$ and the modes considered are those at low frequency because this constitutes the most complex case in terms of accuracy in the estimation of $|k_i|$ (see Fig. 3).

Fig. 13 shows the value of $|k_i|$ for the modes at about 89 (Figs. 13a and c) and 139 Hz (Figs. 13b and d) for the first and third patches when the position of the brick is moved from location deB to deC and deF. The repeatability of the results is good and the associated scatter is not able to hide the differences (when present) among the different locations of the brick. Compare, as an

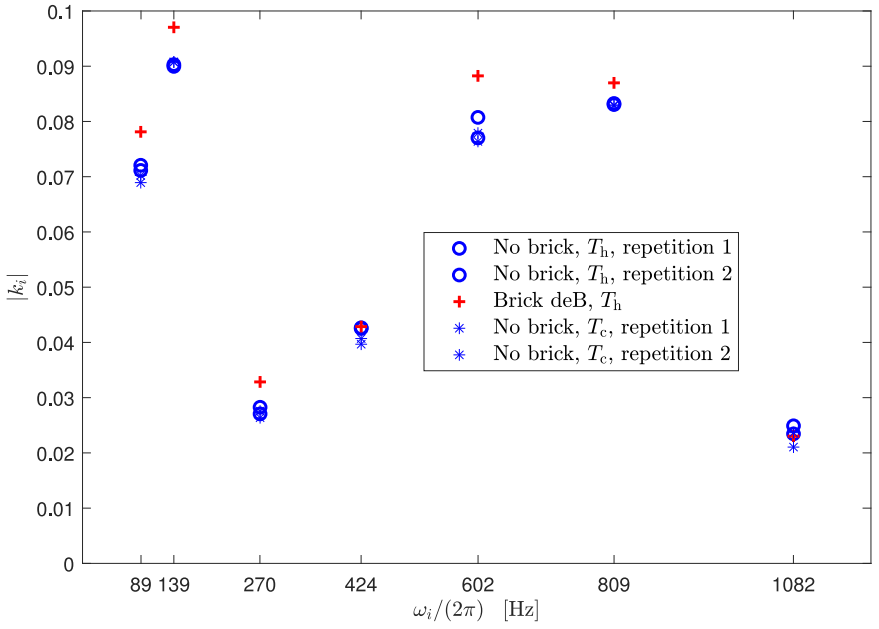

Fig. 12. Experimental $|k_i|$ values identified in different conditions for patch 1 (see Fig. 10b).

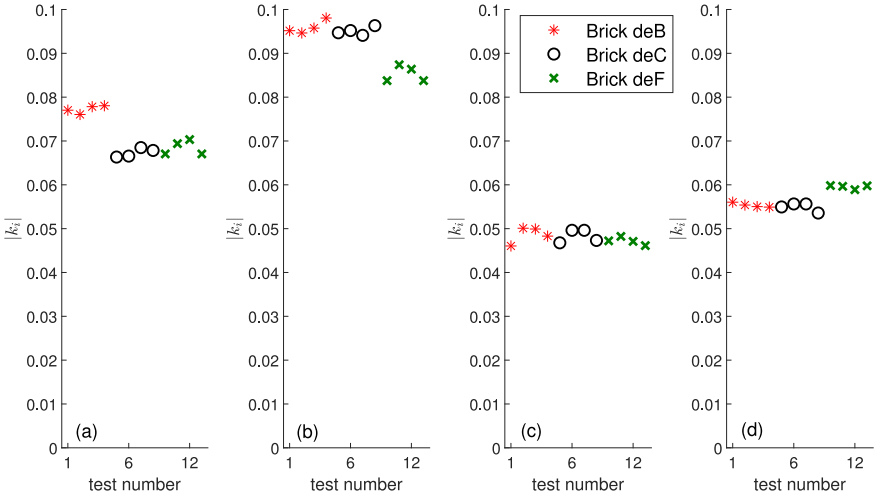

Fig. 13. $|k_i|$ values with the brick in locations deB, deC and deF for the mode at about 89 Hz and the first patch (a), the mode at about 139 Hz and the first patch (b), the mode at about 89 Hz and the third patch (c) and the mode at about 139 Hz and the third patch (d). Refer to Fig. 10b.

example, the results for brick in locations deB and deF in Fig. 13d. In this case, non-significant changes are detected when moving from position deB to deC, both far from the transducer number 3. When, instead, the brick is moved closer to transducer 3, in position deF, the value of $|k_i|$ changes, as expected. However, it is evident that the scatter (and thus the uncertainty) of the results needs to be decreased if small changes of $|k_i|$ should be detected. This can be obtained using an NC, as explained in Section 3 and discussed further in this subsection. Fig. 13 also shows that the brick location has different effects on different modes and between two different patches. $|k_i|$ of, e.g., mode at 89 Hz shows changes for patch 1 (see Fig. 13a) and does not change for patch 3 (see Fig. 13c) when moving from deB to deC. Similarly, considering patch 3, just the mode at 139 Hz is affected by the change of the brick position.

Fig. 14 shows a comparison between experimental results and numerical simulations in terms $\Delta_{i,p}$ for the first patch in correspondence of the mode at about 89 Hz, chosen as an example. There is a good accordance between experiments and simulations and only a slight bias is evidenced for location deB. This slight bias could be caused by the fact that a single experimental $|k_i|$ value was estimated for the non-altered condition.

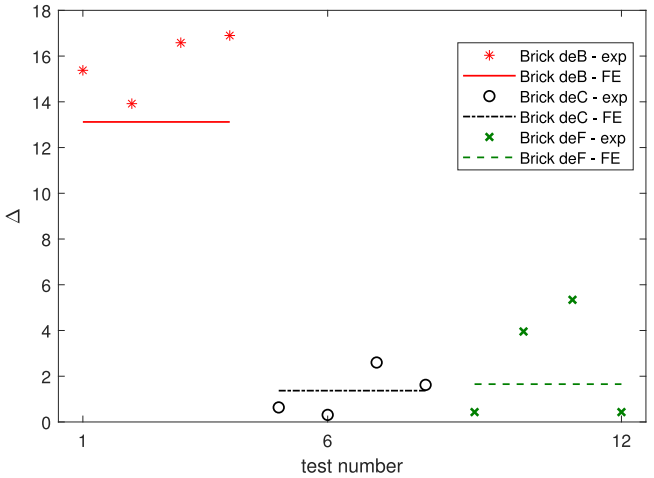

Fig. 14. $\Delta_{i,p}$ values with the brick in locations deB, deC and deF for the mode at about 89 Hz and the first patch: comparison between experimental and FE results.

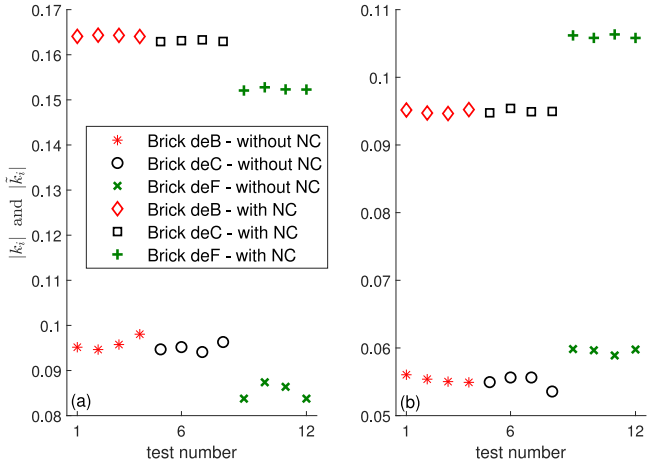

Fig. 15. $|k_i|$ and $|\tilde{k}_i|$ values as functions of the brick location for the mode at approximately 139 Hz and the first patch (a) and for the third patch (b), see Fig. 10b. $|k_i|$ refers to the tests without the NC, while $|\tilde{k}_i|$ refers to the tests with the NC.

Finally, Fig. 15 shows the effect of the NC. In this case the temperature was $T = T_h$ and an NC in series connection was used. Therefore, the value of C_n was set higher than C_0 (see Section 3.1). The value of the C_n was set approximately equal to 134 nF, while C_0 was estimated close to 90 nF [24] for both patches 1 and 3. The NCs were built using OPA445 operational amplifiers supplied with a constant voltage of ±30 V. Refer to [22,47] for more details about how to build an NC. It is evident that the addition of the NC offers two main advantages:

1. the difference between the coupling factor measured in altered and unaltered conditions is larger and easier to detect when the NC is used;
2. the scatter of the results is less relevant because of the decreased uncertainty allowed by the use of the NC. This last result is in agreement with the discussion of Sections 3.1 and 3.2 which showed that the use of $|\tilde{k}_i|$ in place of $|k_i|$ (with $|\tilde{k}_i| > |k_i|$) allows for a reduction of the uncertainty. Therefore, the use of NCs involves a significant improvement in terms of method reliability.

7.1.2. Tests for the use of the index s

These tests were carried out to the purpose of showing the capability of the index s to detect the presence of a structural alteration and also its capability to provide information related to the location.

The tests were performed supposing to work on a limited number of modes because this is a challenging situation. Therefore, the external broadband excitation was provided such that only five bending modes were forced (excitation between 350 and 900 Hz approximately). Some FRFs are provided as examples in Fig. 11c.

Table 3
Details for the tests with patch 1 (refer to Fig. 10b) both with and without the NC.

Test ID	Time	Notes
T1	day 1, afternoon	no brick
T2	day 1, afternoon	no brick
T3	day 1, afternoon	no brick
T4	day 1, evening	brick in deA
T5	day 1, evening	brick in deA
T6	day 2, morning	no brick
T7	day 2, morning	no brick
T8	day 2, morning	brick in deD
T9	day 2, morning	brick in deD
T10	day 2, morning	no brick
T11	day 2, morning	no brick
T12	day 2, morning	brick in deE
T13	day 2, morning	brick in deE
T14	day 2, afternoon	no brick
T15	day 2, afternoon	no brick
T16	day 2, afternoon	brick in deD
T17	day 2, afternoon	brick in deD
T18	day 2, evening	brick in deE
T19	day 2, evening	brick in deE
T20	day 3, morning	no brick
T21	day 3, morning	brick in deA
T22	day 3, morning	brick in deA

Table 4
Details for the tests with patch 3 (refer to Fig. 10b) without employing the NC.

Test ID	Time	Notes
T23	day 4, afternoon	no brick
T24	day 4, afternoon	brick in deA
T25	day 4, evening	brick in deD
T26	day 4, evening	brick in deE
T27	day 5, morning	no brick
T28	day 5, morning	brick in deA
T29	day 5, afternoon	brick in deD
T30	day 5, afternoon	brick in deE

Temperature was left uncontrolled during the experimental activity, with consequent thermal shifts of approximately 6 K. The tests discussed here were carried out both with and without an NC (with C_n set close to 115 nF in this case) for patches number 1 and 3 and the brick was placed in locations deA, deD and deE (see Fig. 10b). Therefore, both patches 1 and 3 are either close to or far from the alteration. Different test repetitions were carried out in different days, as explained in Table 3 for patch 1 and Table 4 for patch 3. At first, the trend of $|k_i|$ and $|\tilde{k}_i|$ values for some of the considered modes will be presented in order to evidence significant facts useful to understand the behaviour of the index s. Fig. 16 shows the identified $|k_i|$ and $|\tilde{k}_i|$ values (see Eqs. (9) and (13)) for two modes and the first patch. The horizontal solid lines evidences the span between the minimum and maximum obtained $|k_i|$ values for the tests without any alteration and not using the NC. The horizontal dashed lines indicate the same type of information for the tests using NC and, thus, for the observed values of $|\tilde{k}_i|$. It must be underlined that these thresholds are not calculated as functions of percentiles of the obtained distributions and that a more detailed analysis will be carried out in future works considering a more rigorous statistical approach. Nevertheless, these thresholds are enough at this first stage of the analysis to show that the presence of the alteration can be detected.

Before analysing the test results and showing the sensitivity of the approach to system alterations, it is worth spending few words about the variability of the considered damage feature (i.e., $|k_i|$) when the system is in the reference unaltered condition. To this purpose, Fig. 16 shows with red asterisks and circles the values of $|k_i|$ and $|\tilde{k}_i|$, respectively, for the modes at 560 and 730 Hz, for patch 1 when the system is in unaltered condition. These tests were carried out in different days and times: T1 to T3 were performed sequentially during the afternoon of day 1, T6, T7, T10 and T11 in the morning of day 2, T14 and T15 in the afternoon of day 2, and T20 in the morning of the third day (see Table 3). Thus, during these tests, the whole temperature range of 6 K was faced. Despite this thermal variability, the scatter of $|k_i|$ can be ascribed to the uncertainty associated to its estimation rather than to the changes of temperature. Indeed, looking at tests T6, T7, T10 and T11 in Fig. 16a, it is possible to notice that, although they were all carried out during the same morning and thus with no relevant temperature change, the estimated $|k_i|$ values span in the whole variability band. This suggests a negligible temperature effect in the whole experimental campaign. A similar conclusion can be drawn for $|\tilde{k}_i|$ values in, e.g., T1 to T3 in Fig. 16b. Moreover, the comparison of the $|k_i|$ results associated to the two modes considered in Fig. 16 (consider the asterisks related to tests T6, T7, T10 and T11 in Figs. 16a and b) further confirms this hypothesis. The variability

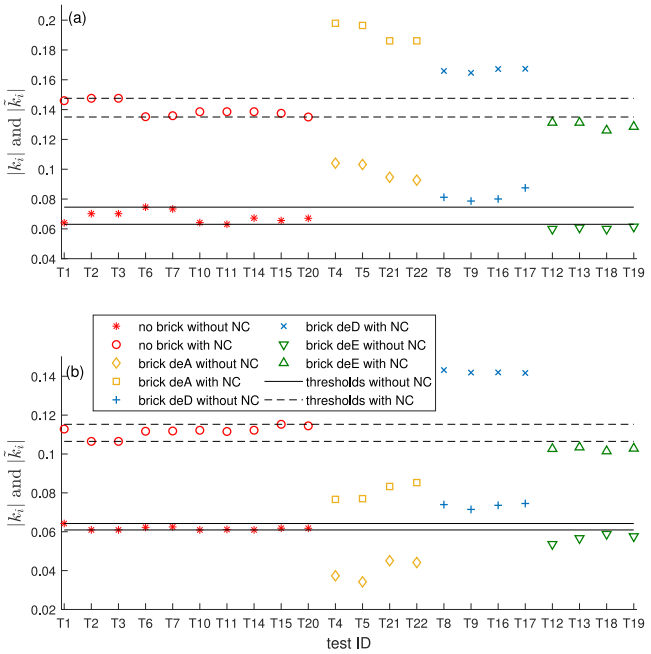

Fig. 16. Experimentally identified values of $|k_i|$ and $|\tilde{k}_i|$ for patch 1 for modes at approximately 560 (a) and 730 Hz (b). The horizontal solid lines evidence span between the minimum and maximum obtained $|k_i|$ values for the tests without any alteration and not using the NC. The horizontal dashed lines indicate the same type of information when using the NC. On the horizontal axis, the first tests are those without the brick, then the tests with the brick in deA, deD and deE are reported. The distance between brick location and patch 1 increases from deA to deE.

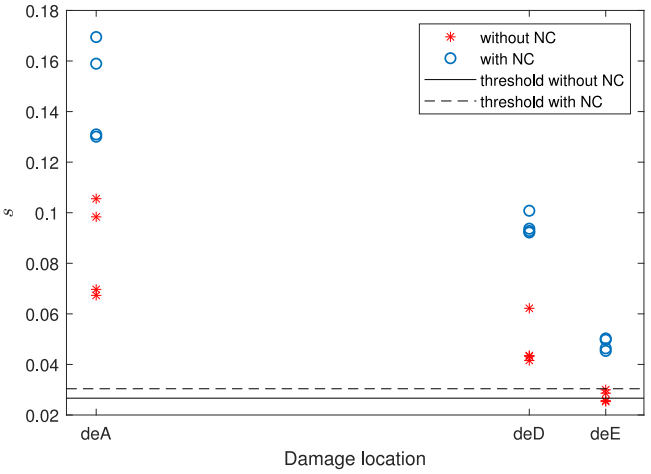

Fig. 17. Experimentally identified s values for patch 1 both with and without the NC.

associated to the estimates of $|k_i|$ for the mode at 730 Hz is indeed lower than that related to the mode at 560 Hz, as expected from the uncertainty analysis of Section 3.2, thus remarking the negligible temperature effect.

It is evident that, most of the times, the alterations close to the considered patch produce changes of either $|k_i|$ or $|\tilde{k}_i|$ outside the thresholds, hinting the possible capability of s to evidence the presence of the alteration. Changes of the $|k_i|$ values for nominally equal conditions can be also evidenced (e.g., see T5 and T21 in Fig. 16a). Here, an additional source of variability is present due to the repetition of the procedure to fix the brick leading to possible inaccuracies in its positioning. Another point that can be evidenced is that the use of an NC allows improving the results, as already evidenced in Section 7.1.1, increasing the distance between results with and without the alteration. Therefore, the use of an NC is expected to provide benefits also when considering the index s.

Then, the index s (see Eq. (11)) was calculated for the different tests described in Tables 3 and 4. Since different tests without the brick were carried out, the reference $|k_i|$ (or $|\tilde{k}_i|$) values of each mode without the brick (to be used in Eq. (11)) were calculated as the mean of the $|k_i|$ (or $|\tilde{k}_i|$) values estimated in the different tests to increase the statistical reliability of the results.

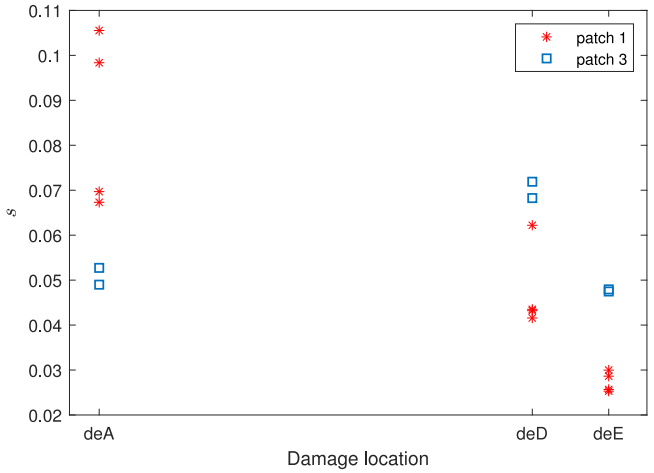

Fig. 18. Experimentally identified s values for patches 1 and 3 without the NC.

The estimated s values are reported in Fig. 17 for tests with patch 1 both without and with the use of the NC. For the calculation of the s values used as references, the mean values of $|k_i|$ (or $|\tilde{k}_i|$) without the alteration were employed, as mentioned. In this way, it was possible to calculate the value of s also for tests without the alteration and the largest obtained values were chosen as thresholds reported as horizontal solid and dashed lines (again, a statistical approach to define the threshold should be used for more accurate results).

The first important point to be underlined is that the index s allows detecting the presence of the alteration because, in all the tests with the brick, the resulting s values are over the thresholds. Few exceptions exist, related to the case in which the brick position is the farthest from the patch and the NC is not employed (see the red asterisks at deE location in Fig. 17). Using the NC, this problem is solved and the presence of the alteration is always clearly detected. It is also noticed that the scatter of the results for the same location of the brick is partly due to the fact that the brick was repositioned on the beam every time and, thus, its position was slightly different every time, as already mentioned.

Moreover, the test results confirm that the patch closest to the alteration is that resulting more sensitive to the presence of the brick. Indeed, even if most of the times the alteration is detected by both the patches regardless their position, the first patch results more sensitive to an alteration in location deA, while the third to alterations in locations deD and deE, as evidenced in Fig. 18.

In summary, the index s allows for the detection of the alteration and the use of an NC enables to improve the sensitivity of the method to the alteration enhancing its detection capability even when the alteration is not close to the patch employed for estimating s. Finally, the use of more than one patch, coupled to the estimation of s for all of them, also allows obtaining information about the location of the alteration.

7.2. Tests with a truss

A more complex test rig was then considered to test the method feasibility in a real-like structure with a real damage and hint the method potentiality. The structure was a steel truss (see Fig. 19a) with length equal to 1 m, characterised by three main pillars with external diameter equal to 15 mm and thickness to 2 mm. The crossbeams are 160 mm long and have an external diameter of 5 mm. The connection between the main pillars and the ground is usually obtained by means of three steel spacers. In this set-up two of them were replaced by piezoelectric stack actuators (type PI P-212.20 with length of 60 mm and made from PIC 255 material) for the purpose of controlling the vibration associated to the first bending modes of the truss. In these tests, the two stacks were instead used to the purpose of monitoring the structure. More specifically, five bending modes were monitored and they are evidenced in Fig. 20, where the FRF of the undamaged truss is presented with all the stacks short-circuited, and then with one of them open-circuited. The disturbance to the truss was provided by a contactless actuator based on a coil (see Fig. 19b) and was of random nature. The horizontal force exerted by this actuator was assumed as proportional to the current flowing in the coil [71] and measured with a current clamp. The horizontal structural response was measured with two accelerometers (PCB Piezotronics, type 333B30) placed on the top and measuring in orthogonal directions. The FRFs in Fig. 20 are quite close in frequency at the considered modes, implying small $|k_i|$ values and making more challenging their estimation through Eq. (9). For this reason, before applying any damage to the truss, the undamaged configuration was tested also in short-circuit with the addition of an NC in series with the aim of improving the accuracy of the coupling estimates, as explained in Section 3. Fig. 21 shows the magnification on three modes among those evidenced in Fig. 20, highlighting that the addition of an NC allows working with larger values of $|\tilde{k}_i|$ and thus lowering the uncertainty on their estimation. The value of C_n was set approximately equal to 115 nF, while C_0 was estimated close to 105 nF [24] for both the stacks. The NCs connected to the two stacks were built using again OPA445 operational amplifiers.

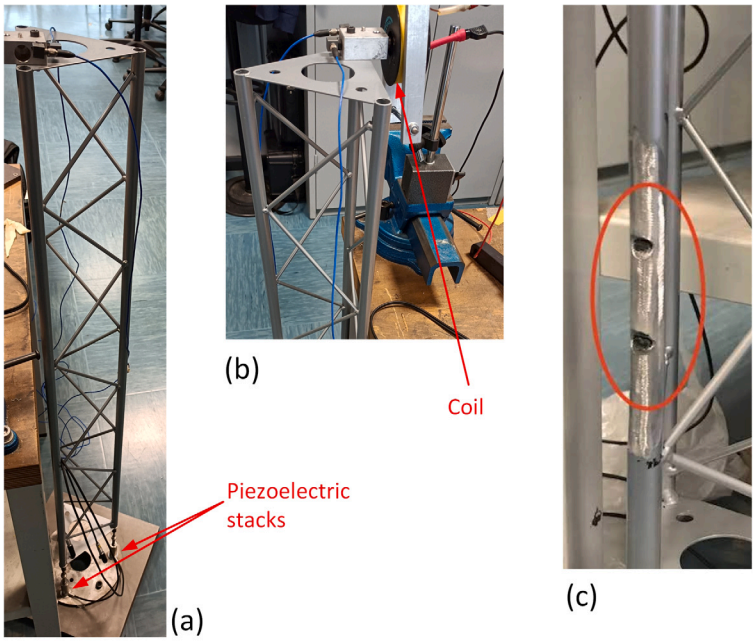

Fig. 19. The truss structure (a), the contactless actuator (b) and the damage (c).

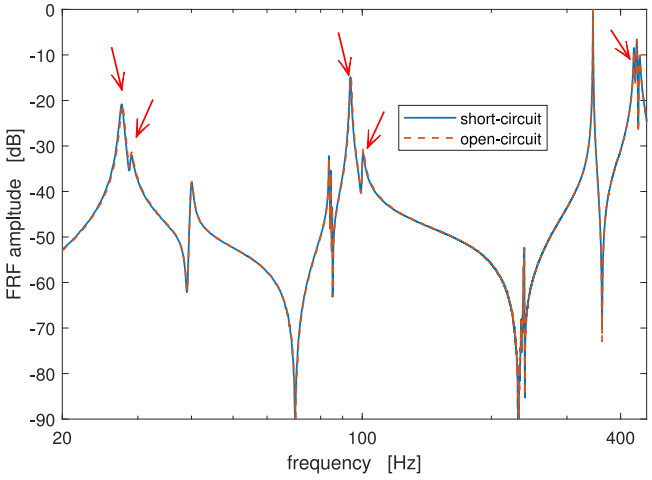

Fig. 20. The FRF of the truss between the external disturbance provided by the contactless actuator and one of the accelerometers with both the stacks short-circuited (without NC) and then with one of them open-circuited. The red arrows indicate the five modes considered for the monitoring.

Since there are two pairs of coupled modes (see Fig. 20), the signals from the two accelerometers were used in each eigenfrequency identification stage to correctly assign the eigenfrequencies to the associated modes by using the modal assurance criterion [69].

The damage was obtained by milling one of the main pillars in two close places (see Fig. 19c), approximately 20 cm above the piezoelectric stacks. The height of the cuts was of few millimeters and led to a decrease of total mass of less than 0.12% (estimated by weighting). The limited loss of mass is also proved by the slight change of eigenfrequency values for the five bending modes considered (see Table 5).

Fig. 22 shows the trend of $|\tilde{k}_i|$ for both the stacks. The first stack (plot (a)) is not able to evidence the presence of the cuts because the $|\tilde{k}_i|$ values in the damaged and undamaged situations are too close, leading to an s value close to 0.02. Conversely, the damage can be easily evidenced by considering the change of the $|\tilde{k}_i|$ values in correspondence of the first two modes for the second stack (plot (b)). The global s value calculated in this case on the five modes is approximately equal to 0.17.

This evidences that the approach is feasible also in case of complex structures and also on limited frequency ranges. Obviously, in this case it is not possible to test the relationship between the position of the stacks and of the damage because the two stacks are at the same height (at ground in this case). Future tests will allow for analysing how the distance between the stack and the damage affects the trend of the $|\tilde{k}_i|$ values.

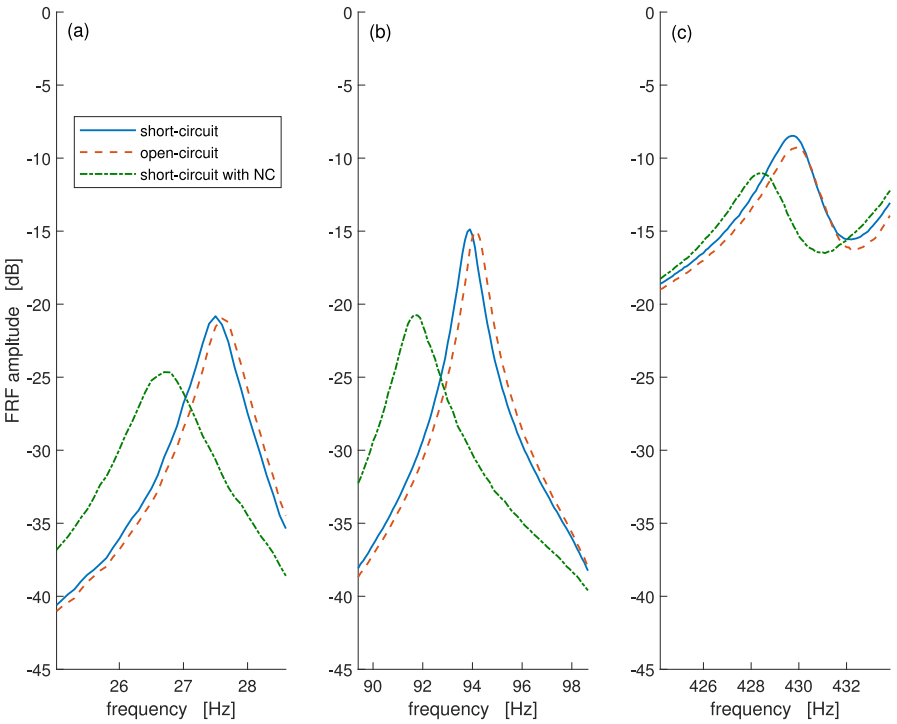

Fig. 21. The FRF of the truss between the external disturbance provided by the contactless actuator and one of the accelerometers with both the stacks short-circuited (without NC), and then with one of them open-circuited and short-circuited with an NC. The three subplots are magnifications on three different modes among those evidenced by the arrows in Fig. 20.

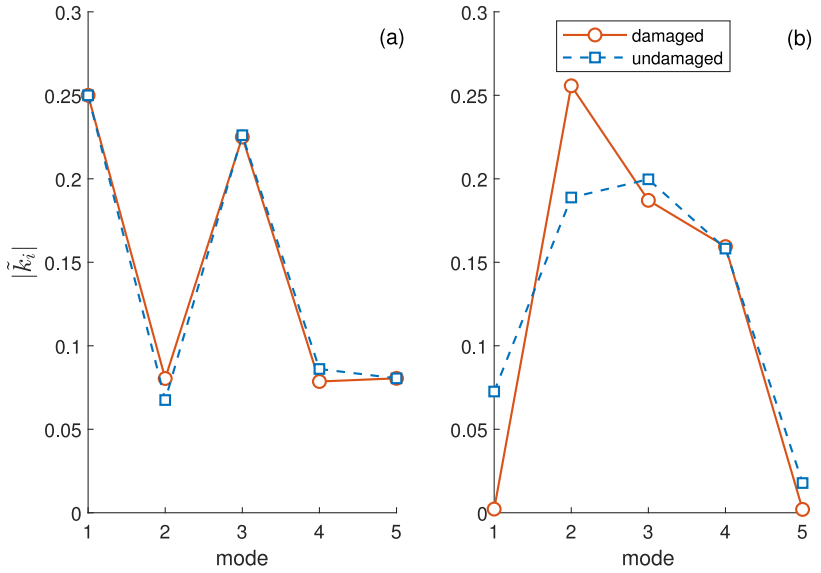

Fig. 22. Trends of $|\tilde{k}_i|$ for the modes evidenced in Fig. 20 in undamaged and damaged conditions: first (a) and second (b) stack transducer.

8. Main strengths of the use of electro-mechanical coupling for SHM purposes

This section aims at shortly summarising the main characteristics of the newly proposed approach based on the use of the electro-mechanical coupling factor as a damage feature for SHM purposes, which emerged from all the presented analyses. They are listed underneath:

Table 5
Eigenfrequency values (in Hertz) for the considered bending modes of the truss with the stacks short-circuited (without NC).

Undamaged	Damaged
27.79	27.27
29.03	28.78
93.88	92.73
100.71	99.09
429.95	429.95

- the electro-mechanical coupling factor is a quantity dependent on mode shapes but it can be estimated by simply deriving eigenfrequencies. This offers the advantages of SHM methods based on mode shape estimation (or related quantities) but without being affected by their usual problems (e.g., noise effects on estimated mode shapes, dense sensor mesh);
- the estimating procedure is simple, based on well-established methods, requires simple measurement devices, and, when required, its accuracy can be improved by using NCs. Furthermore, it requires to work in the low frequency range, which improves its feasibility;
- the newly proposed damage feature is robust to environmental and operational conditions;
- there is no need of long training;
- there is no need of any model of the system. Even in this condition, it is possible to have also indications about alteration position (when more than one piezoelectric element is used);
- the electro-mechanical coupling factor can be estimated using already available transducers present on the system/structure;
- the damage feature can be estimated with the system/structure under operating conditions and the needed external excitation can be obtained both by providing external actions or exploiting environmental excitation;
- the electro-mechanical coupling factors estimated for different modes can be used either to develop a stand-alone monitoring system or to provide additional information to more complex SHM methods.

9. Conclusions and future developments

The paper has proposed an exploratory study of a new method for detecting structural alterations/changes in light structures. The approach is based on a pattern of piezoelectric transducers coupled to the structure, and uses as damage feature the electro-mechanical coupling. This coupling can be estimated for each transducer by deriving the modal electro-mechanical coupling factors, indirectly measured through eigenfrequency identification. A relevant peculiarity of the approach is that it can also use piezoelectric transducers already available on the structure/system for different purposes, e.g., for vibration control, energy harvesting and micro-positioning. This allows all these systems having an intrinsic monitoring capability, which is valuable especially when no monitoring systems are already present on board.

The proposed analyses were focused on proving the reliability and sensitivity of the approach, rather than comparing its performances with those of other well-established SHM strategies. Indeed, due to its peculiarities, the use of electro-mechanical coupling as damage feature offers some advantages which make the SHM techniques based on it, not only an alternative to other strategies, but also a complementary tool able to enhance the performances of more complex SHM systems. Indeed, being based on differential measurements of the system eigenfrequencies, the electro-mechanical coupling showed good robustness with respect to environmental and operating conditions; its estimate does not require any interruption of the system functioning and relies on robust and well-established modal identification techniques, aimed at evaluating the system eigenfrequencies. This entails a system which does not require any expensive or complex device. Moreover, despite a deepened analysis about the method sensitivity and accuracy was not presented in this paper, the reliability and robustness of the approach was shown being easily improved by shunting NCs to the transducers, giving the method a high adaptation capability to face different scenarios (e.g., either large or small initial $|k_i|$ values). All these aspects make the proposed damage feature also a good input for already existing monitoring systems/algorithms, aimed at facilitating and improving their functioning.

The feasibility of the approach was tested both numerically and experimentally. The experimental tests were carried out on two test-case structures and the results confirmed the feasibility and effectiveness of the proposed approach. Since the proposed analyses were aimed only at investigating the possibility of using modal electro-mechanical coupling factor measurements for SHM, there are still several aspects which deserve a thorough analysis. First and foremost, the optimisation of the size and position of the transducers deserves a more detailed insight in order to comprehend the maximum level of sensitivity to alterations/damages that can be reached. Indeed, although both the simulations and the experiments, where the piezoelectric elements were not optimised in terms of size and location on the structure, showed good results, these aspects can improve the method performances and the smallest detectable alteration. Concerning this latter aspect, also the effect of the environmental factors on the uncertainty related to the damage identification needs to be assessed. Therefore, the feasibility study proposed here paves the way to thorough studies aimed at consolidating the use of modal electro-mechanical coupling factor measurements to detect structural alterations.

CRediT authorship contribution statement

M. Berardengo: Writing – review & editing, Writing – original draft, Validation, Supervision, Resources, Project administration, Methodology, Investigation, Funding acquisition, Formal analysis, Conceptualization. **M. Brambilla:** Visualization, Software, Investigation, Data curation, Writing – review & editing. **A. Codina:** Validation, Software, Methodology, Investigation, Formal analysis, Data curation. **N. Schena:** Visualization, Validation, Software, Investigation, Data curation. **S. Manzoni:** Writing – original draft, Visualization, Supervision, Resources, Methodology, Investigation, Funding acquisition, Formal analysis, Conceptualization, Writing – review & editing.

Declaration of competing interest

The authors declare that they have no known competing financial interests or personal relationships that could have appeared to influence the work reported in this paper.

Data availability

Data will be made available on request.

Acknowledgements

This research has been supported by the project "CHIMERA? - is there a CHance that Indexes and Measurements of the energy conversion Efficiency Reveal system Alterations?" funded by the European Union – Next Generation EU, M4C2 I1.1, through Progetti di Rilevante Interesse Nazionale (PRIN), grant n. 20225PKHWJ (CUP: D53D23003060006).

References

[1] R. Hou, Y. Xia, Review on the new development of vibration-based damage identification for civil engineering structures: 2010–2019, J. Sound Vib. 491 (2020) 115741, http://dx.doi.org/10.1016/j.jsv.2020.115741.
[2] S. Hou, C.S. Cai, J. Ou, Seismic damage identification for steel structures using distributed fiber optics, Appl. Opt. 48 (22) (2009) 4483–4489.
[3] D. Dessi, G. Camerlengo, Damage identification techniques via modal curvature analysis: Overview and comparison, Mech. Syst. Signal Process. 52–53 (1) (2015) 181–205, http://dx.doi.org/10.1016/j.ymssp.2014.05.031.
[4] J.-T. Kim, N. Stubbs, Improved damage identification method based on modal information, J. Sound Vib. 252 (2) (2002) 223–238.
[5] C.P. Ratcliffe, A frequency and curvature based experimental method for locating damage in structures, Journal of Vibration and Acoustics 122 (3) (2000) 324–329.
[6] M. Cao, M. Radzienski, W. Xu, W. Ostachowicz, Identification of multiple damage in beams based on robust curvature mode shapes, Mech. Syst. Signal Process. 46 (2) (2014) 468–480, http://dx.doi.org/10.1016/j.ymssp.2014.01.004.
[7] C. Rodrigues, C. Júnior, D. Rade, Application of machine learning techniques and spectrum images of vibration orbits for fault classification of rotating machines, J. Control, Automat. Electr. Syst. 33 (1) (2022) 333–344, http://dx.doi.org/10.1007/s40313-021-00805-x.
[8] B. Peeters, G. De Roeck, One-year monitoring of the Z24-bridge: Environmental effectsversus damage events, Earthq. Eng. Struct. Dyn. 30 (2) (2001) 149–171, http://dx.doi.org/10.1002/1096-9845(200102)30:2<149::AID-EQE1>3.0.CO;2-Z.
[9] L. Bull, T. Rogers, C. Wickramarachchi, E. Cross, K. Worden, N. Dervilis, Probabilistic active learning: An online framework for structural health monitoring, Mech. Syst. Signal Process. 134 (2019) 106294, http://dx.doi.org/10.1016/j.ymssp.2019.106294.
[10] W. Soo Lon Wah, J. Owen, Y.-T. Chen, A. Elamin, G. Roberts, Removal of masking effect for damage detection of structures, Eng. Struct. 183 (January) (2019) 646–661, http://dx.doi.org/10.1016/j.engstruct.2019.01.005.
[11] S. Allahdadian, M. Döhler, C. Ventura, L. Mevel, Towards robust statistical damage localization via model-based sensitivity clustering, Mech. Syst. Signal Process. 134 (2019) http://dx.doi.org/10.1016/j.ymssp.2019.106341, Article ID: 106341.
[12] D. Giagopoulos, A. Arailopoulos, V. Dertimanis, C. Papadimitriou, E. Chatzi, K. Grompanopoulos, Structural health monitoring and fatigue damage estimation using vibration measurements and finite element model updating, Struct. Health Monit. 18 (4) (2019) 1189–1206, http://dx.doi.org/10.1177/1475921718790188.
[13] K. Padil, N. Bakhary, M. Abdulkareem, J. Li, H. Hao, Non-probabilistic method to consider uncertainties in frequency response function for vibration-based damage detection using artificial neural network, J. Sound Vib. 467 (2020) http://dx.doi.org/10.1016/j.jsv.2019.115069, Article ID: 115069.
[14] V. Giurgiutiu, A. Zagrai, J. Bao, Damage identification in aging aircraft structures with piezoelectric wafer active sensors, J. Intell. Mater. Syst. Struct. 15 (9–10) (2004) 673–687, http://dx.doi.org/10.1177/1045389X04038051.
[15] J. Zhao, J. Tang, Amplifying damage signature in periodic structures using enhanced piezoelectric networking with negative resistance elements, J. Intell. Mater. Syst. Struct. 24 (13) (2013) 1613–1625, http://dx.doi.org/10.1177/1045389X13479184.
[16] F. Sun, Z. Chaudhry, C. Liang, C. Rogers, Truss structure integrity identification using PZT sensor-actuator, J. Intell. Mater. Syst. Struct. 6 (1995) 134–139, http://dx.doi.org/10.1177/1045389X9500600117.
[17] F. Zahedi, H. Huang, Time – frequency analysis of electro- mechanical impedance (EMI) signature for physics-based damage detections using piezoelectric wafer active sensor (PWAS), Smart Mater. Struct. 26 (2017) 055010, http://dx.doi.org/10.1088/1361-665X/aa64c0.
[18] D.E. Budoya, L.M. Campeiro, F.G. Baptista, Sensitivity enhancement of piezoelectric transducers for impedance-based damage detection via a negative capacitance interface, IEEE Sens. J. 20 (23) (2019) 13892–13900, http://dx.doi.org/10.1109/jsen.2019.2956782.
[19] M. Berardengo, S. Manzoni, M. Brambilla, M. Vanali, A. Codina, The use of piezoelectric coupling in structural monitoring as a feature robust to EOV, in: Proceedings of the 11th European Workshop on Structural Health Monitoring (EWSHM 2024), June 10-13, 2024, Potsdam (Germany) and Special Issue of E-Journal of Nondestructive Testing (EJNDT) ISSN 1435-4934, 2024.
[20] V. Giurgiutiu, Structural health monitoring of aerospace composites, Academic Press, 2016.
[21] O. Thomas, J. Ducarne, J. Deü, Performance of piezoelectric shunts for vibration reduction, Smart Mater. Struct. 21 (1) (2012) 015008.
[22] M. Berardengo, O. Thomas, C. Giraud-Audine, S. Manzoni, Improved resistive shunt by means of negative capacitance: new circuit, performances and multi mode control, Smart Mater. Struct. 25 (2016) 075033.

[23] J. Toftekær, J. Høgsberg, Multi-mode piezoelectric shunt damping with residual mode correction by evaluation of modal charge and voltage, J. Intell. Mater. Syst. Struct. 31 (4) (2019) 570–586.
[24] M. Berardengo, S. Manzoni, J. Høgsberg, M. Vanali, Vibration control with piezoelectric elements: The indirect measurement of the modal capacitance and coupling factor, Mech. Syst. Signal Process. 151 (2021) 107350, http://dx.doi.org/10.1016/j.ymssp.2020.107350.
[25] J. Ducarne, O. Thomas, J. Deü, Placement and dimension optimization of shunted piezoelectric patches for vibration reduction, J. Sound Vib. 331 (14) (2012) 3286–3303.
[26] M. Berardengo, S. Manzoni, M. Vanali, The behaviour of mistuned piezoelectric shunt systems and its estimation, Shock Vib. 2016 (2016) 9739217.
[27] M. Berardengo, A. Cigada, S. Manzoni, M. Vanali, Vibration control by means of piezoelectric actuators shunted with LR impedances: Performance and robustness analysis, Shock Vib. 2015 (2015) 704265.
[28] M.D. Ulriksen, L. Damkilde, Structural damage localization by outlier analysis of signal-processed mode shapes - analytical and experimental validation, Mech. Syst. Signal Process. 68–69 (2016) 1–14, http://dx.doi.org/10.1016/j.ymssp.2015.07.021.
[29] Y. Shokrani, V. Dertimanis, E. Chatzi, M. Savoia, On the use of mode shape curvatures for damage localization under varying environmental conditions, Struct. Control Health Monit. 25 (4) (2018) http://dx.doi.org/10.1002/stc.2132.
[30] M. Dahak, N. Touat, M. Kharoubi, Damage detection in beam through change in measured frequency and undamaged curvature mode shape, Inverse Probl. Sci. Eng. 27 (1) (2019) 89–114, http://dx.doi.org/10.1080/17415977.2018.1442834.
[31] N.M. Maia, J.M. Silva, E.A. Almas, R.P. Sampaio, Damage detection in structures: From mode shape to frequency response function methods, Mech. Syst. Signal Process. 17 (3) (2003) 489–498, http://dx.doi.org/10.1006/mssp.2002.1506.
[32] J. Ciambella, A. Pau, F. Vestroni, Modal curvature-based damage localization in weakly damaged continuous beams, Mech. Syst. Signal Process. 121 (2019) 171–182, http://dx.doi.org/10.1016/j.ymssp.2018.11.012.
[33] A. Preumont, Mechatronics: Dynamics of Electromechanical and Piezoelectric Systems, Springer, 2006.
[34] S. Chesne, C. Jean-Mistral, L. Gaudiller, Experimental identification of smart material coupling effects in composite structures, Smart Mater. Struct. 22 (2013) http://dx.doi.org/10.1088/0964-1726/22/7/075007, article ID: 075007.
[35] M. Porfiri, C. Maurini, J. Pouget, Identification of electromechanical modal parameters of linear piezoelectric structures, Smart Mater. Struct. 16 (2) (2007) 323–331, http://dx.doi.org/10.1088/0964-1726/16/2/010.
[36] B. Zhou, F. Thouverez, L. D., Vibration reduction of mistuned bladed disks by passive piezoelectric shunt damping techniques, AIAA J. 52 (2014) 1194–1206, http://dx.doi.org/10.2514/1.J052202.
[37] K. Zhou, Z. Hu, Stochastic vibration suppression of composite laminated plates based on negative capacitance piezoelectric shunt damping, Thin-Walled Struct. 180 (2022) 109802, http://dx.doi.org/10.1016/j.tws.2022.109802.
[38] H. Sun, Z. Yang, K. Li, B. Li, J. Xie, D. Wu, L. Zhang, Vibration suppression of a hard disk driver actuator arm using piezoelectric shunt damping with a topology-optimized PZT transducer, Smart Mater. Struct. 18 (2009) http://dx.doi.org/10.1088/0964-1726/18/6/065010, article ID: 065010.
[39] G. Raze, A. Paknejad, G. Zhao, C. Collette, G. Kerschen, Multimodal vibration damping using a simplified current blocking shunt circuit, J. Intell. Mater. Syst. Struct. 31 (14) (2020) 1731–1747, http://dx.doi.org/10.1177/1045389X20930103.
[40] W.P. Li, H. Huang, Integrated optimization of actuator placement and vibration control for piezoelectric adaptive trusses, J. Sound Vib. 332 (1) (2013) 17–32, http://dx.doi.org/10.1016/j.jsv.2012.08.005.
[41] M. Sabatini, G. Palmerini, P. Gasbarri, Synergetic approach in attitude control of very flexible satellites by means of thrusters and PZT devices, Aerosp. Sci. Technol. 96 (2020) 105541, http://dx.doi.org/10.1016/j.ast.2019.105541.
[42] L. Yan, B. Bao, D. Guyomar, M. Lallart, Structural shape reconstruction of fiber bragg grating flexible plate based on strain modes using finite element method, J. Intell. Mater. Syst. Struct. 28 (2) (2017) 204–229.
[43] R. Darleux, B. Lossouarn, J.-F. Deü, Broadband vibration damping of non-periodic plates by piezoelectric coupling to their electrical analogues, Smart Mater. Struct. 29 (2020) article ID: 054001.
[44] A.K. Pandey, M. Biswas, M.M. Samman, Damage detection from changes in curvature mode shapes, J. Sound Vib. 145 (2) (1991) 321–332.
[45] P. Horowitz, W. Hill, The art of electronics, second ed., Cambridge University Press, 1989.
[46] B. de Marneffe, A. Preumont, Vibration damping with negative capacitance shunts: theory and experiment, Smart Mater. Struct. 17 (3) (2008) 035015.
[47] M. Berardengo, S. Manzoni, O. Thomas, M. Vanali, Piezoelectric resonant shunt enhancement by negative capacitances: optimisation, performance and resonance cancellation, J. Intell. Mater. Syst. Struct. 29 (12) (2018) 2581–2606.
[48] M. Berardengo, S. Manzoni, O. Thomas, C. Giraud-Audine, A new electrical circuit with negative capacitances to enhance resistive shunt damping, in: Proceedings of the ASME 2015 Conference on Smart Materials, Adaptive Structures and Intelligent Systems - SMASIS 2015 - September 21-23, 2015 - Colorado Springs (CO, USA), 2015.
[49] M. Berardengo, O. Thomas, C. Giraud-Audine, S. Manzoni, Improved shunt damping with two negative capacitances: an efficient alternative to resonant shunt, J. Intell. Mater. Syst. Struct. 28 (16) (2017) 2222–2238.
[50] JCGM, Evaluation of measurement data - guide to the expression of uncertainty in measurement, 2008, 2008, JCGM 100:2008.
[51] H. Shi, K. Worden, E. Cross, A regime-switching cointegration approach for removing environmental and operational variations in structural health monitoring, Mech. Syst. Signal Process. 103 (2018) 381–397, http://dx.doi.org/10.1016/j.ymssp.2017.10.013.
[52] H. Sarmadi, A. Entezami, B. Saeedi Razavi, K. Yuen, Ensemble learning-based structural health monitoring by mahalanobis distance metrics, Struct. Control Health Monit. 28 (2021) http://dx.doi.org/10.1002/stc.2663, Article ID: e2663.
[53] A. Entezami, H. Sarmadi, M. Salar, C. De Michele, A. Arslan, A novel data-driven method for structural health monitoring under ambient vibration and high-dimensional features by robust multidimensional scaling, Struct. Health Monit. (2021) http://dx.doi.org/10.1177/1475921720973953.
[54] F. Cadini, L. Lomazzi, M. Ferrater Roca, C. Sbarufatti, M. Giglio, Neutralization of temperature effects in damage diagnosis of MDOF systems by combinations of autoencoders and particle filters, Mech. Syst. Signal Process. 162 (2021) http://dx.doi.org/10.1016/j.ymssp.2021.108048, article ID: 108048.
[55] A. Entezami, H. Sarmadi, S. Mariani, Early damage assessment in large-scale structures by innovative statistical pattern recognition methods based on time series modeling and novelty detection, Adv. Eng. Softw. 150 (2020) 102923, http://dx.doi.org/10.1016/j.advengsoft.2020.102923.
[56] M. Berardengo, F. Lucà, M. Vanali, G. Annesi, Short-training damage detection method for axially loaded beams subject to seasonal thermal variations, Sensors 23 (3) (2023) 1154, http://dx.doi.org/10.3390/s23031154.
[57] J. Berntsen, A. Brandt, Periodogram ratio based automatic detection and removal of harmonics in time or angle domain, Mech. Syst. Signal Process. 165 (2022) 108310, http://dx.doi.org/10.1016/j.ymssp.2021.108310.
[58] K. Worden, G. Manson, N. Fieller, Damage detection using outlier analysis, J. Sound Vib. 229 (3) (2000) 647–667, http://dx.doi.org/10.1006/jsvi.1999.2514.
[59] E. Figueiredo, G. Park, C. Farrar, K. Worden, J. Figueiras, Machine learning algorithms for damage detection under operational and environmental variability, Struct. Health Monit. 10 (6) (2011) 559–572, http://dx.doi.org/10.1177/1475921710388971.
[60] C. Rainieri, G. Fabbrocino, Operational Modal Analysis of Civil Engineering Structures, Springer, 2014.
[61] L. Avendaño-Valencia, E. Chatzi, D. Tcherniak, Gaussian process models for mitigation of operational variability in the structural health monitoring of wind turbines, Mech. Syst. Signal Process. 142 (2020) http://dx.doi.org/10.1016/j.ymssp.2020.106686, article ID: 106686.
[62] W. Na, J. Baek, A review of the piezoelectric electromechanical impedance based structural health monitoring technique for engineering structures, Sensors 18 (2018) http://dx.doi.org/10.3390/s18051307, article ID: 1307.
[63] G. Park, H. Sohn, C. Farrar, D. Inman, Overview of piezoelectric impedance-based health monitoring and path forward, The Shock and Vibration Digest 35 (2003) 451–463, http://dx.doi.org/10.1177/05831024030356001.

[64] G. Park, H. Cudney, D. Inman, An integrated health monitoring technique using structural impedance sensors, J. Intell. Mater. Syst. Struct. 11 (2000) 448–455, http://dx.doi.org/10.1106/QXMV-R3GC-VXXG-W3AQ.
[65] D. de Souza Rabelo, V. Steffen Jr., R. Finzi Neto, H. Lacerda, Impedance-based structural health monitoring and statistical method for threshold-level determination applied to 2024-T3 aluminum panels under varying temperature, Struct. Health Monit. 16 (4) (2017) 365–381, http://dx.doi.org/10.1177/1475921716671038.
[66] B. Lossouarn, L. Rouleau, R. Darleux, J.-F. Deü, Comparison of passive damping treatments based on constrained viscoelastic layers and multi-resonant piezoelectric networks, J. Struct. Dyn. (1) (2021) 30–48, http://dx.doi.org/10.25518/2684-6500.63.
[67] C. Dumoulin, A. Deraemaeker, A study on the performance of piezoelectric composite materials for designing embedded transducers for concrete assessment, Smart Mater. Struct. 27 (3) (2018) http://dx.doi.org/10.1088/1361-665X/aaa7fe, article ID: 035008.
[68] www.piceramic.com, PI Ceramic.
[69] A. Brandt, Noise and Vibration Analysis – Signal Analysis and Experimental Procedures, second ed., Wiley, 2023.
[70] H. Van der Auweraer, P. Guillaume, P. Verboven, S. Vanlanduit, Application of a fast-stabilizing frequency domain parameter estimation method, J. Dyn. Syst. Measur. Control Trans. ASME 123 (4) (2001) 651–658, http://dx.doi.org/10.1115/1.1410369.
[71] O. Thomas, C. Touzé, A. Chaigne, Asymmetric non-linear forced vibrations of free-edge circular plates. part II: experiments, J. Sound Vib. 265 (5) (2003) 1075–1101.